Reaction dynamics of H_2 and D_2 on Si(100) and Si(111)

2001 J. Phys.: Condens. Matter 13 R61

(http://iopscience.iop.org/0953-8984/13/9/201)

INSTITUTE OF PHYSICS PUBLISHING JOURNAL OF PHYSICS: CONDENSED MATTER

J. Phys.: Condens. Matter **13** (2001) R61–R94 www.iop.org/Journals/cm PII: S0953-8984(01)13840-3

TOPICAL REVIEW

Reaction dynamics of H_2 and D_2 on Si(100) and Si(111)

W Brenig and M F Hilf

Physik-Department, Technische Universität München, D-85747 Garching, Germany

Received 26 June 2000

Abstract

Experimental and theoretical results on the dynamics of dissociative adsorption and recombinative desorption of hydrogen molecules on silicon are reviewed.

The temperature dependence of the desorption rates for H_2 and D_2 on Si(100) and Si(111) corresponds to a desorption barrier of 2.3–2.4 eV. Adsorption is phonon assisted: the sticking coefficient increases strongly with surface temperature, corresponding to an activation energy of 0.65 eV at a gas temperature of 300 K (with little isotope effect). It also increases with incident gas energy. The adsorption barrier is strongly reduced by the presence of defects and steps on the surface and by preadsorbed H atoms at inter-dimer positions. The barrier *at steps*, for instance, is only of the order of 0.1 eV. The state-resolved energetics of the desorbing particles shows an excess energy (including translational energy) above thermal which is small compared to the activation barrier to adsorption. The angular dependence of sticking and desorption is strongly forward peaked ($\propto(\cos\theta)^{10\,\mathrm{to}\,11}$ or $\propto(\cos\theta)^{3\,\mathrm{to}\,4}$ depending on azimuth).

Molecular vibrations show vibrational *heating* in desorption (with a strong isotope effect) and vibrationally assisted sticking at higher temperatures. On the other hand, molecular rotations show *cooling* in desorption.

Ab initio generalized gradient approximation slab calculations for the H_2 interaction with the dimers of Si(100)2 $\times$ 1 and with the Si 'adatoms' on Si(111)7 $\times$ 7 all indicate the existence of strong lattice relaxations near the adsorption sites and the transition state geometries in qualitative agreement with the observed phonon-assisted sticking. The energetically lowest transition state on Si(100) is the inter-dimer state which also has the highest elastic relaxation energy (about 0.33 eV). The barrier of the asymmetric intra-dimer state is slightly higher but the relaxation energy is only half as big. There is also a symmetric intra-dimer transition state with an even higher barrier. It may, nevertheless, contribute to sticking and desorption due to a large phase space.

The slab calculations yield good values for the desorption barrier heights of 2.3 to 2.5 eV. They also lead to a good semiquantitative understanding of the existence of highly reactive sites near steps and preadsorbed H atoms at inter-dimer states. The absolute values of adsorption barriers, however, come out consistently too low by about 0.2 to 0.4 eV. Since in our review we are not so much interested in pursuing the consequences of *ab initio* calculations in detail but more in a model describing the experimental data quantitatively, we

allow ourselves to readjust the *ab initio* results slightly to obtain good fits to the data. Because of the uncertainties of the *ab initio* results, the relation of model parameters to the various transition states is uncertain as well.

The strong phonon assistance of sticking can be modelled fairly well by taking only a single lattice displacement coordinate at the adsorption site into account. Together with the six degrees of freedom of the molecule, one obviously needs a model with at least seven degrees of freedom. We will present a seven-dimensional Hamiltonian which we treat in a seven-dimensional time-independent coupled-channel calculation. The results of this calculation agree well with experimental data. Most of the results are more or less independent of the particular transition state mediating the reaction. An exception, perhaps, is the angular dependence of sticking coefficients and desorption fluxes. We discuss several alternatives for explaining the observed angular distributions in terms of possible transition states.

1. Introduction

The interaction of hydrogen with silicon surfaces has been the focus of extensive experimental [1–13, 17–20] and theoretical [21–43, 45, 46, 48] efforts. There are two excellent review articles, concerning H_2/Si directly [50] or in the context of other *ab initio* dynamical calculations [51]. In our review we concentrate on recent experiments relevant to dynamical aspects of adsorption and desorption and their detailed quantum mechanical description in terms of models and *ab initio* calculations.

The great interest in the subject is, of course, partly due to the importance of H/Si in semiconductor chemistry [52, 53]. Equally important, however, is that hydrogen on silicon is a promising model system for studying general aspects of chemical reactions on covalent surfaces. It may be expected that the localized nature of the bonding on semiconductor surfaces will give rise to a reaction behaviour that is in many respects qualitatively different from that for metal surfaces.

One consequence of the localized nature of H–Si bonds, e.g., is the large diffusion barriers that were observed experimentally for H/Si(111)7×7 [5] and have been predicted theoretically for H/Si(100)2×1 [23, 26, 32]. Also, the finding that the kinetics of desorption of H_2 from silicon depend on the details of the surface reconstruction [4, 6] is due to the local character of Si–H chemisorption.

Another rather dramatic manifestation of the localized nature of hydrogen interaction with silicon surfaces is the occurrence of strong lattice distortions during adsorption/desorption of molecular hydrogen on/from Si(111)7×7 and Si(100)2×1. The dynamics of these distortions provides the solution of the so-called 'barrier puzzle' resulting from state-resolved experiments on hydrogen desorption from silicon surfaces [10, 12, 28]: it has been known for many years that the room temperature sticking coefficient of molecular H_2 on silicon surfaces is very low, less than 10^{-6}–10^{-8} [54–56]. This indicates the presence of a high adsorption barrier of $V_{ads} > 0.5$ eV. However, the energetics of desorbing molecules, in particular the low translational energy of desorbing molecules [12], seems to indicate the absence of a substantial potential drop during desorption. This is, for instance, quite different from the situation for H_2/Cu where the adsorption barrier leads to a strong translational heating of desorbing hydrogen molecules.

Lattice relaxation is frequently associated with adsorption [57] and may influence adsorption/desorption barriers even for metal surfaces [58]. In the case of H/Si, theoretical investigations indicate that the diffusion [23, 32, 35] and desorption barriers [22] decrease substantially when the Si atoms relax. However—concerning the barrier puzzle—a model involving *only static* lattice distortion of silicon between the two states that are 'hydrogen adsorbed' and 'hydrogen desorbed' (and a corresponding barrier change) would lead to a violation of detailed balance [12, 34]. This stimulated the first quantum mechanical coupled-channel calculation for the reaction dynamics of H_2/Si introducing a new scenario into the adsorption/desorption arena: up to then it had been considered that there are mainly two mechanisms for dissipating the energy in an adsorption process:

(a) For *non-dissociative* processes (atomic and molecular adsorption), energy transfer to the substrate (phonons and/or electrons) is the dominant effect.
(b) For *dissociative* adsorption, just conversion of centre-of-mass energy into internal molecular energy, in particular kinetic energy, was assumed to be sufficient.

H_2/Si seems to be the first example where both energy-transfer processes have to be taken into account on an equal footing.

In the absence of a detailed *ab initio* potential energy surface (PES), a simple two-dimensional model was proposed for studying such reactions [34]. It contained—besides the centre-of-mass distance of the molecule from the surface—only a single additional coordinate, namely the amplitude of a 'representative surface oscillator', associated with lattice distortions. The shape of the PES used in [34] was modelled to describe existing experimental facts, in particular the absence of translational heating in spite of a high barrier to adsorption. This was achieved by (i) assuming an approximately constant potential contour for *zero* lattice displacement starting on the barrier and (ii) a rather short-ranged potential drop in the centre-of-mass coordinate for the *asymptotic* lattice displacement (corresponding to hydrogen in the gas phase). In this way, the centre-of-mass coordinate feels little force along the reaction path during desorption. The dominant coupling is to the lattice coordinate. Conditions (i) and (ii) lead to a PES circumventing to some extent Polanyi's rules [59] for the usual 'curved' reaction paths which normally produce translational heating together with vibrational heating in exothermic processes.

A pseudo-3D plot is depicted in figure 1 of reference [34] (see also section 3). Such a potential obviously leads to a strong lattice excitation in desorption without significant translational heating. Application of time reversal to such a desorption process then leads to a large sticking coefficient for an *excited lattice*. Hence, such a model predicts strong *phonon-assisted sticking*.

Experimentally, such a strong enhancement of the sticking probability was indeed observed, first for H_2 adsorption on Si(111)7×7 [7] and then also for Si(100)2×1 [8]. In these experiments, it was possible to measure sticking coefficients of the order of 10^{-9} by a technique based on optical second-harmonic generation (SHG).

In section 2 of the present paper, we give a more detailed description of these adsorption experiments. Experiments on the isotope dependence of sticking as well as desorption, and results on the coverage dependence of the sticking coefficient on the Si(111)7×7 surface further corroborate our previous conclusions from the observation of phonon-assisted sticking [7, 8]. It is the strong lattice distortion in the transition state, as modelled by our PES, that is the dominant mechanism leading to the observed 'asymmetry' between dissociative adsorption and recombinative desorption.

More recently [89], adsorption experiments have been performed combining supersonic molecular beam techniques and optical second-harmonic generation. They indicate a rather

strong increase of the sticking coefficient $s(E)$ with the translational energy E of the incident beam. This is in semiquantitative agreement with the 2D model described above. Detailed quantitative agreement, however, could only be achieved by making a slight change of parameters, leading to some translational heating in desorption. This is intimately connected with the principle of detailed balance and rather independent of the details of the model used. There is now some discrepancy between the early results on absence of translational heating in desorption and recent data on $s(E)$: if we use these data to fix our parameters, the two conditions (i) and (ii) described above for reducing translational heating in desorption have to be relaxed somewhat. This leads to some force on the centre of mass in adsorption/desorption and an energy of desorbing molecules which is about twice the thermal energy. Since this energy is still small compared to the height of the barrier to adsorption, the general picture is not changed substantially.

The original 2D model has meanwhile been extended to seven dimensions to include the effect of surface corrugation, molecular vibrations and rotations. The main effect of corrugation is a reduction of the sticking coefficient by up to an order of magnitude depending slightly on temperature and on the corrugation parameters. Also, the angular distribution of desorption and adsorption becomes more forward peaked as a result of corrugation. Molecular vibrations have little effect on the adsorption/desorption dynamics itself but lead to vibrational heating in desorption with a strong isotope effect and vibrationally assisted sticking at higher temperatures. The rotational degrees of freedom show rotational cooling in desorption associated with the release of rotational frustration and another decrease of the pre-exponential in the sticking coefficients by about a factor of two. Apart from the slight inconsistencies between adsorption and desorption experiments as regards the translational energy transfer, the 7D models seem to be able to describe all currently available experimental data.

Recently, the influence of steps and defects on the Si(100) surface on the reaction dynamics of hydrogen has been investigated [95]. The effect is rather dramatic: adsorption barriers are reduced by an order of magnitude. In these experiments the influence of doping concentration on sticking at Si(001) has also been determined. It turned out that doping levels up to 10^{19} cm^{-2} do not affect the reaction kinetics.

Ab initio calculations for the PES for the interaction of H_2 with the Si–Si dimers of the Si(100) and the Si(111) surfaces can be divided into two classes.

GGA slab calculations [36, 38, 46, 86] agree qualitatively with the results obtained from the 2D model PES. They yield good values for the *desorption* barrier but somewhat too small values for the adsorption barrier of and for the amount of coupling to the lattice for Si(100). They also yield valuable additional information for this surface concerning the other degrees of freedom which can be used in the 7D calculations.

Cluster calculations (see e.g. [25, 40, 43]) lead to desorption barriers which are usually about 1 eV too high, with the exception of those from [40], but to reasonable adsorption barriers.

Both slab and cluster calculations predict strong anisotropies in the angular dependence of the desorption and sticking probabilities. Experimentally [18], the desorption probability is strongly forward peaked. Also, recently measured angular dependencies of sticking coefficients show no anisotropies, indicating more symmetric transition states than the *ab initio* calculations.

Recently, *ab initio* calculations concerning the influence of steps at the Si(001) surfaces on the reaction dynamics were also carried out [97, 98]. It turned out that the double-atomic-height rebonded D_B step which is known to be stable on the clean surface remains stable on partially hydrogen-covered surfaces. The rebonded Si atoms on the step show buckling similar to that of the 'clean' surface. For monohydride formation from a molecule approaching the

rebonded atoms parallel to the step, one finds essentially no barrier. So this path seems to be responsible for the observed increase in sticking coefficients.

More recently, inter-dimer reaction paths have also been investigated experimentally [94, 95] and theoretically [99]. Exposing clean surfaces to hydrogen, one finds using a scanning tunnelling microscope adsorbed hydrogen at inter-dimer sites for low coverages and low temperatures. *Ab initio* calculations indicate that there are reaction pathways towards such states with even lower barriers than towards intra-dimer states.

Furthermore, it turns out that hydrogen adsorbed between two dimer ends produces highly reactive sites at the other end. The situation is analogous to the high reactivity of step sites on Si(100) vicinal surfaces.

2. Experiment

In this section we present a brief review of experimental results. We concentrate mainly on those data which are relevant for our dynamic theory. Plots of the data will be presented only later on, together with results of dynamic calculations.

We distinguish three groups of experiments.

2.1. Group 1

We begin with *state-resolved desorption* data [10–13]. They contain important information concerning the behaviour of the molecular degrees of freedom during the reaction, such as vibrational heating, rotational cooling and in particular a translational energy distribution close to thermal. The latter result together with the existence of a large dissociation barrier led to the so-called 'barrier puzzle', stimulating many further theoretical and experimental investigations.

There are also data on angular distributions of desorbing molecules [18] exhibiting non-thermal (forward-peaked) distributions.

2.2. Group 2

A second group of experiments concerns sticking coefficients of *gaseous hydrogen* on Si(100) and Si(111) as a function of surface and gas temperature [7–9].

The extremely small sticking coefficients for dissociative adsorption of H_2/Si were measured using optical second-harmonic generation (SHG) [7]. For pump wavelengths near 1 μm this technique is very sensitive to the number of Si dangling bonds. It allows the determination of small hydrogen coverages with a sensitivity that exceeds that of most conventional techniques. The lowest sticking coefficients measured in this way were of the order of 10^{-9}. This high sensitivity has already been exploited in making accurate measurements of H_2 desorption kinetics [4, 6] and surface diffusion of H/Si [5]. Using the compatibility of SHG with any gas pressure, it was possible to measure the H coverage directly during exposure of the surface to a high flux of molecular H_2. In this way, it is possible to measure sticking coefficients for dissociative adsorption even for surface temperatures that exceed the H_2 desorption temperature. At these temperatures, the desorption rates could also be measured. The activation energies for desorption were all between $E_d = 2.3$ and 2.4 eV, in good agreement with previous isothermal SHG, laser-induced thermal desorption and temperature-programmed desorption experiments. Furthermore, the coverage dependence of the sticking coefficient results directly from these experiments.

The sticking coefficients exhibit an activated dependence on surface temperature with an activation energy between $E_a = 0.7$ eV for H_2, D_2/Si(100) and $E_a = 0.9$ eV for D_2/Si(111). The pre-exponential factors are of the order of $10^{-(1\,\mathrm{to}\,2)}$.

2.3. Group 3

More recently the *sticking of molecular beams* has been investigated [89]. The translational energy dependence of sticking coefficients turned out to be stronger than expected from the earlier model calculations. The parameters of these models were fixed so as to describe the absence of translational heating. The new data now indicate a translational heating of desorbing molecules to about twice the thermal value. The angular distribution of desorbing particles then would be expected to be strongly forward peaked. Similarly the sticking coefficient can be expected to have a corresponding angular dependence. Such a dependence has, indeed, been observed [93].

3. *Ab initio* calculations of the potential

In this section we will present a short review of *ab initio* calculations of the hydrogen–silicon PES.

3.1. The cluster model

Early attempts [21,22,24,29–31] used a *cluster model* for the Si surface. The cluster approach was continued with bigger clusters and varying methods [23, 25, 26, 40, 44, 83]. The results of this approach are described in great detail by Doren [50] so we allow ourselves to be brief. The cluster calculations have stimulated interesting discussions about the influence of dimers, monohydrides and dihydrides, the so-called 'pre-pairing' mechanism and defect-mediated desorption. Usually the cluster calculation yields a large excess energy of the transition state residing in the H–H stretch, predicting strong vibrational heating. Attempts to explain the barrier puzzle in terms of this prediction rather than lattice distortions [44] suffer from an improper treatment of zero-point-energy contributions in comparing classical molecular dynamics with experiment [51]. They are also not in accord with the observed absence of an isotope effect in the desorption rates.

With the exception of those of [40], all cluster calculations yield desorption barriers which are substantially (by about 1 eV or more) too high. The reasons for the exception are discussed in [50]: the calculation of [40] differs strongly from prior cluster calculations by involving geometry optimization without constraints. We take this as an indication that barriers in cluster models are very sensitive to the conditions imposed at the surface, casting doubts on the usefulness of such models for quantitative purposes. The most detailed investigation of the dependence of cluster-derived results [87] on the cluster size indicates that for H_2/Si(100), only from sizes as large as $Si_{21}H_{20}$ on do the results become comparable to slab data. Cluster data may still yield useful qualitative insights and interesting results concerning the comparison of different approximation methods and functionals using DFT, but even these results may depend on cluster sizes.

3.2. Slab calculations

Fortunately, meanwhile there have been several attempts to establish a microscopic picture from density functional *slab calculations* for hydrogen on Si(100)2 $\times$ 1 [36, 38] and on

Si(111) [46, 85, 86]. It has been proposed that the most important process of hydrogen interaction with Si(100)2 × 1 is the interaction of both hydrogen atoms with a *single Si–Si dimer* on the Si(100)2 × 1 surface [2, 3, 6, 27]. Together with the pre-pairing of the hydrogen atoms on these dimers, this mechanism provides a natural explanation for the observed first-order desorption kinetics. The asymmetry between dissociative adsorption and recombinative desorption on Si(100) arises because the silicon dimers are found to be horizontally oriented when hydrogen is adsorbed [3, 82], whereas they are buckled on the clean surface [78–80]. Since the buckling is accompanied by charge transfer within the dimer and a rehybridization of orbitals in the two silicon atoms [78, 81], there is a notable dependence of the H_2 adsorption barrier on the buckling angle [36, 38].

3.3. The 'adatom' of the 7 × 7 *reconstructed surface*

On Si(111), hydrogen adsorption/desorption is associated also with a strong lattice distortion in the vicinity of the so-called *'adatom' of the* 7 × 7 *reconstructed surface* [39, 46, 86]. In [9] a strong 'back-bond stretching' in the transition state was proposed on heuristic grounds. This assumption was verified by DFT *ab initio* slab calculations [86] and an adsorption barrier of 0.8 eV was found, slightly higher than the observed value. Also, qualitative arguments were presented for the absence of substantial translational heating. Since, however, the translational energy in desorption is small compared to the barrier height, it depends on small details of the PES which have not been calculated so far. So a real microscopic reason for the absence of translational heating in desorption from Si(111) going beyond our model calculations is still awaited.

In contrast to the cluster results, the slab calculations yield desorption barriers close to the experimental values (2.4 eV). On the other hand, adsorption barriers come out somewhat too low (0.4 eV instead of 0.65 eV) for on Si(100). In this comparison one has to bear in mind, however, that the experimental value is for low coverage and the theoretical one for high coverage. If the experimental value is extrapolated linearly to high coverage (using the observed coverage dependence), one finds a value of 0.55 eV which agrees better with the *ab initio* results.

3.4. The symmetric transition state

One should also keep in mind that the calculated values are for the asymmetric transition state. There is, however, also a *symmetric transition state* [36] with a barrier about 0.2 eV higher in energy. The symmetric state is 'softer', leading to larger pre-exponentials. So this state may well contribute substantially to the adsorption/desorption dynamics.

The detailed structure of the *ab initio* PES of Si(100) is slightly different from the model PES: the *ab initio* dynamics yields too much translational heating of the desorbing hydrogen (in spite of a barrier which is too low for on Si(100)). Discrepancies between calculated and measured values of translational energies are, however, only of the order of 0.1 eV. This is an indication of the sensitivity of the translational energy to subtle details of the PES: the accuracy of present-day *ab initio* results (about 0.1 eV) usually gives a rather good account of equilibrium data. Barrier heights usually come out less well. Molecular beam data, in particular state-resolved results, are, generally speaking, still an order of magnitude more accurate.

The *ab initio* PES contains a potential drop of about 0.2 eV with increasing centre-of-mass distance of hydrogen from the surface at constant lattice coordinate of the unbuckled dimer. This leads to an energy difference between the buckled and unbuckled dimer states of the clean surface of about 0.2 eV in agreement with experiment. On the other hand, it leads to

an increased translational heating as compared to our model potential. If the model potential were to be corrected to describe the observed asymptotic behaviour of the clean surface, a corresponding correction at small z would have to be introduced. For instance, an additional curvature of the reaction path could bend the desorption trajectories away from the potential drop and reduce translational heating. In order to avoid too many additional parameters, we have, so far, not considered such modifications of our potential presented in the next section.

3.5. Steps and defects

Stimulated by the recent experiments [95] concerning the influence of *steps and defects* on adsorption barriers, DFT slab calculations were performed for vicinal Si(001) surfaces [98]. Under the experimental conditions, double-atomic-height steps prevail on the surface having additional threefold-coordinated Si atoms attached to the step edges, the so-called rebonded D_B steps. The bond length of these atoms is extended. According to the DFT results the hydrogen dissociation proceeds via two neighbouring rebonded atoms which are buckled similarly to the dimers on the terraces.

The huge decrease in adsorption barrier height arises from the interplay of lattice relaxation and electronic structure effects. The electronic structure at the step is different from the one on the ideal surface dimer reconstruction: the two surface bands formed from the localized dangling bonds at the step may come rather close in energy (0.4 eV) because the step-edge Si atoms have no common bond and interact only weakly. Upon approach of molecular hydrogen, these surface states can rehybridize and thus interact efficiently with the hydrogen orbitals. On the other hand, the distance of the two Si atoms on the Si dimers at the ideal surface is smaller; hence the π-interaction of the dangling bonds is stronger and prevents the two surface-band centres from coming closer than 0.7 eV. Therefore the terrace sites are less capable of dissociating hydrogen molecules.

The above interpretation of adsorption by step-mediated processes predicts a saturation at full monohydride coverage of the steps, in agreement with experiment.

The calculated adsorption barrier at steps is actually zero. Before comparing this value with the observed 0.09 eV, a detailed dynamical calculation has to be done including further degrees of freedom such as molecular vibrations and corrugation. One also has to keep in mind that the barrier on the terrace comes out between 0.1 and 0.2 eV too low. Taking this into account, the results for the stepped versus clean surfaces further corroborate the interpretation of adsorption/desorption on the terraces as occurring on (buckled) dimers on Si(100) rather than as defect-mediated events.

3.6. Inter-dimer reaction paths

As mentioned in the introduction, *inter-dimer reaction paths* have been investigated experimentally [94, 95] and theoretically [39, 99]. Exposing clean surfaces to hydrogen, one finds using a scanning tunnelling microscope adsorbed hydrogen at inter-dimer sites for low coverages and low temperatures. *Ab initio* calculations first indicated [39] that the reaction pathways towards such states had barriers somewhat higher than for the intra-dimer states. More careful consideration of lattice relaxation for the inter-dimer states, however, led to even lower barriers than for intra-dimer states [99]. Lattice relaxation energies for the inter-dimer states come out about twice as large (0.3 eV) as for the inter-dimer situation.

Furthermore, it turns out that hydrogen adsorbed between two dimer ends produces highly reactive sites at the other end. The high reactivity is explained as being due to dangling-bond states close to the Fermi level which can efficiently hybridize with the anti-bonding state of

the hydrogen molecule. This is analogous to the high reactivity of step sites on Si(100) vicinal surfaces discussed above.

4. The 7D Hamiltonian

In this section we present a 7D model Hamiltonian to be used in our dynamic calculations. We first introduce the variables in terms of which we will describe the potential energy surface (PES) and then present a few general comments concerning the choice of variables and potentials.

4.1. Coordinates

As a first step we express the cartesian coordinates of the two hydrogen atoms $Z_{1,2}$ and $\boldsymbol{Y}_{1,2}$ in terms of the centre of mass z, $\boldsymbol{y}$ and relative coordinates, and the relative coordinates in terms of the H–H distance r and polar angles ϑ, φ: $Z_{1,2} = z \pm r(\cos\vartheta)/2$ and $\boldsymbol{Y}_{1,2} = \boldsymbol{y} \pm r \sin\vartheta(\cos\varphi, \sin\varphi)/2$.

In order to describe dissociation we introduce the usual *reaction path coordinates* (s, v) [62–65] instead of the original (z, r). The so-called reaction coordinate s asymptotically approaches z in the gas phase and the H–H distance r in the adsorbed phase. The vibration coordinate v describes the H–H stretch vibrations in the gas phase and the H–Si stretch on the surface. A key quantity in the reaction path coordinate system is the *curvature* $C(s)$ of the reaction path in the original system. It occurs in the *Jacobian*

$$\eta(s) = 1 - C(s)v \tag{1}$$

of the transformation.

4.2. Coupling

The substrate to be taken into account is, of course, a strongly coupled many-body system. The coupling to the molecule will be simplified by making use of the short range of the H–Si interaction and of the timescales involved in the adsorption/desorption reaction. The direct H–Si coupling will involve only very few atoms: a single one in a head-on collision of the incident molecule, or two atoms of a single dimer, or of two dimer neighbours. The vibrational amplitudes of these atoms can be written as linear combinations of surface modes being excited strongly in the first instance of a desorption process. We assume that there is essentially only one such mode which dominates the lattice response initially and call its amplitude x.

The consideration of only a single mode is justified *a posteriori* by classical lattice dynamics for Si(100) taking 32 atoms into account [48]: it turns out that for low temperatures immediately after desorption only one atom of the dimer involved in adsorption/desorption has an appreciable oscillation amplitude. Later on the energy of this atom, of course, is dissipated into other degrees of freedom. But this has no strong influence on the adsorption probability any more as soon as the hydrogen has left the transition region. At higher temperatures, other degrees of freedom are excited (even before adsorption/desorption), but this essentially corresponds to a Boltzmann distribution of the substrate superimposed onto the low-temperature situation.

4.3. Asymptotics

A corresponding simplification will be used concerning the *static* H–Si interaction on the surface side of the transition region. Our simplified model will be complete only on the gas

side. On the surface side we will assume that the periodic potentials acting on the centre of mass of the molecule in the transition region drop to zero on the surface side like on the gas side. Concerning the relative motion of the adsorbed hydrogen atoms, we will assume only harmonic vibrations perpendicular and parallel to the surface.

The quantum numbers of the asymptotic states after adsorption (or before desorption) can then be chosen rather similarly to the asymptotic states in the gas phase. One has two parameters (identical to those for the gas phase): E (total energy) and $\boldsymbol{Q} = 2\pi\hbar(n_1, n_2)/L$ (total momentum parallel to the surface; the n_i are integral numbers for periodic boundary conditions within L), and four discrete ones $\boldsymbol{m} = (m_p, m_v, m_1, m_2)$ for the phonons, and the H vibrations perpendicular or parallel to the surface. They may be compared to total energy and momentum E and $\boldsymbol{P}$ as well as $\boldsymbol{n} = (n_p, n_v, l, m)$ for phonons, molecular vibrations and rotations in the gas phase.

While the asymptotic states in the gas phase exist physically for long times, the corresponding states on the surface side exist only as transient 'first intermediates' in the adsorption or 'last intermediates' in the desorption process. The physically asymptotic states long after adsorption or before desorption are the quasi-equilibrium states of adsorbed hydrogen plus substrate. Our model can only describe desorption *from* and adsorption *into* the intermediates. In order to eliminate unobservable details of the intermediates, one considers sticking probabilities *summed* over and desorption probabilities *averaged* over the quantum numbers of the intermediates. We assume that the coupling of the intermediates to the physically asymptotic states leads to Boltzmann equilibrium of the intermediates but otherwise does not influence the adsorption/desorption rates.

4.4. The Hamiltonian in the new variables

We are now in a position to express the Hamiltonian $H = T + V$ in the new variables. We use mass-scaled coordinates and use the mass of the molecule $m = 2m_{\text{proton}}$ as the only explicit mass. Then the kinetic energy can be written as

$$T = -\frac{\hbar^2}{2m}\left(\eta^{-1}\,\partial_s\eta^{-1}\,\partial_s + \partial_v^2 - \eta^{-1}C(s)\,\partial_v + \partial_{\boldsymbol{y}}^2 + \partial_x^2 - \frac{L^2}{r^2(s)}\right). \tag{2}$$

Here $r(s) = \langle r(s, v)\rangle_0$ is the mass-scaled H–H distance, averaged over the vibrational ground state (i.e. we neglect vibrational–rotational coupling).

In principle, the potential can be constructed by an expansion around the reaction path. If we assume that this runs along the minimum $V_t(s)$ of the multidimensional potential function, the first-order terms in the six remaining variables vanish. If the second-order terms are diagonalized, the off-diagonal second-order terms vanish too. We simplify this general procedure by assuming that the potential *is diagonalized already* in the variables x, v, $\boldsymbol{y}$, $\boldsymbol{x}_r$ introduced above ($\boldsymbol{x}_r = \boldsymbol{x}_r(\vartheta, \varphi)$ is the mass-scaled vector from the first hydrogen atom to the second one which was expressed in terms of polar coordinates in subsection 4.1 above). The potential then has the structure

$$V(x, \boldsymbol{y}, v, \boldsymbol{x}_r; s) = V_t(s) + V_p(x; s) + V_v(v; s) + V_r(\vartheta, \varphi; s) + V_c(\boldsymbol{y}; s) \tag{3}$$

where the subscript t stands for translation, p for substrate ('phonon'), v for (molecular) vibrations, r for rotations and c for corrugation.

Note that the structure of the r.h.s. of (3), in particular the additivity in the various degrees of freedom, is not a model assumption depending on the physical meaning of the variables, but just a mathematical consequence of the harmonic approximation.

4.5. Potentials

4.5.1. Translation. The first term $V_t(s)$ (the *translational potential*) then, as just described, gives the value along the *minimum* of the multidimensional potential with respect to the coordinates orthogonal to s, i.e. along the line of steepest descent of the PES. We have chosen the following parametrization:

$$V_t(s) = (V_d - V_a)\frac{\tanh(\lambda s) - 1}{2} + \frac{1}{4}(V_d + V_a + 2\sqrt{V_d V_a})\frac{1}{\cosh^2(\lambda s)} \tag{4}$$

with an adsorption barrier V_a, a desorption barrier of V_d and a potential decay length λ.

The adsorption barrier can be determined so as to yield the observed very low value of the sticking coefficient at room temperature of the order of 10^{-8} leading to $V_a \simeq 0.6$ eV. The desorption barrier V_d is known from experiment [2, 4, 6] to be $V_d = 2.3$ to 2.4 eV. λ has an influence on the translational energy dependence of the sticking coefficient $s(E)$ and on the translational energy in desorption. If one chooses (see the discussion in the introduction) a rather small decay length corresponding to $\lambda = 2.7$ Å^{-1}, the desorbing molecules leave the interaction region quickly and show no translational heating. A somewhat smaller value of $\lambda = 2.0$ Å^{-1} leads to some translational heating and is in better agreement with the recent data on $s(E)$ [89].

The additional four terms describe the coupling of centre-of-mass motion along the reaction path with lattice vibrations, molecular vibrations, rotations and the centre-of-mass motion parallel to the surface. To lowest order the potential is quadratic in the variables x, v, $\boldsymbol{y}$, $\boldsymbol{x}_r$ as assumed in (3).

We now extend the procedure to higher orders by taking anharmonic terms into account. However, rather than considering systematically higher terms in a power expansion, we keep the structure of (3), neglecting off-diagonal terms. We replace the harmonic potential V_p (and V_v if necessary) by Morse potentials and V_c, which is harmonic near the periodically distributed adsorption sites, by a cosine function. In contrast to the harmonic approximation, equation (3) then describes a *model* and is no longer uniquely determined by mathematics.

4.5.2. Phonons (substrate). We introduce the *coupling to the lattice* by assuming an s-dependent shift $\Delta(s)$ of the potential minimum in the form

$$V_p(x; s) = \frac{\hbar\omega_p(s)}{2} d^2 \left(1 - \exp\left(-\frac{x - \Delta(s)}{a_p(s)d}\right)\right)^2. \tag{5}$$

The phonon potential depth is expressed in terms of d^2, the number of bound states, which we fix at $d^2 = 39$ independently of s. The oscillator length is $a_p(s) = \sqrt{\hbar/M^*\omega_p(s)}$ with the frequency $\hbar\omega_p(s) = E_1(s) - E_0(s)$ defined as the quantum of the first excited state.

We choose the effective phonon mass M^* to be the mass of a single Si atom, and for the frequency we use the parametrization

$$\hbar\omega_p(s) = \hbar\omega_g + (\hbar\omega_g - \hbar\omega_s)\big(\tanh(\lambda_p(s - s_p)) - 1\big). \tag{6}$$

For the frequency with H in the gas phase, we use $\omega_g = 45$ meV. The latter is a mean of the values for several optical modes [37, 66, 67]. At the barrier ($s = s_p$) we take a frequency smaller than that by a factor of two with a smooth interpolation on the length scale λ_p between this and the asymptotic value.

The results of the dynamical calculations are not very sensitive to the parameters of the Morse potential. On the other hand, the shift $\Delta(s)$ has a strong influence on the translational energy in desorption and on the translational energy dependence of the sticking coefficient $s(E)$. If one wants to minimize translational heating, one can do this by ensuring a 'straight'

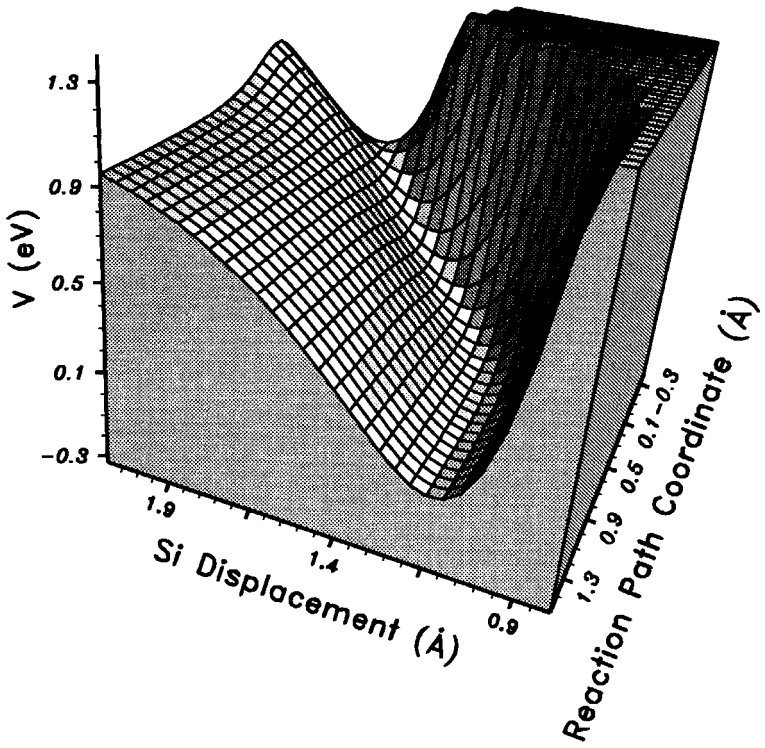

Figure 1. A 3D plot of the dependence of the PES on the silicon displacement x and reaction coordinate s. Note the strong shift of the minimum with s leading to a strong translation–phonon coupling.

(independent of z) constant-potential contour on the 'gas side' of the potential starting at the top of the barrier. On the other hand, if one wants to have a stronger increase of $s(E)$ with E in order to fit the recent molecular beam data, one has to relax this condition somewhat, allowing for some potential drop in the z-direction after the barrier and a corresponding translational heating.

We use the parametrization

$$\Delta(s) = \Delta_0\{[1 + \tanh(\lambda_d(s - s_d))]/2\}^7 \tag{7}$$

which is smooth at the barrier and has some additional flexibility via the choice of λ_d and s_d. For the results in section 4 we used $\Delta_0 = 0.55$ Å, $\lambda_d = 2.7$ Å^{-1} and $s_d = -0.15$ Å. Figure 1 shows the phonon potential.

4.5.3. Vibration. The *molecular vibration* dynamics leaves the adsorption/desorption dynamics of the model calculations presented above essentially unchanged (apart from zero-point-energy contributions to the PES). This is obvious from the small amount of energy transferred into the intra-molecular degree of freedom. Although the population of the first excited state of the desorbing molecule at a surface temperature of 780 K is about a factor of 20 higher than for thermally equilibrated molecules, the difference in average vibrational energy is merely about 6 meV for H_2, 10 meV for HD and 25 meV for D_2.

Nevertheless, the vibrational dynamics of the molecules including their isotope effect is interesting in itself. The coupling of the molecular vibrations is produced by an s-dependent

stretching of the intra-molecular bond length leading to an elbow-like curved reaction path [62]. As pointed out already, one transforms to a locally orthogonal coordinate system (v, s) in order to apply the coupled-channel method, placing the potential minimum at $v = 0$ [75].

Because of the low molecular vibrational energy produced in the reaction, it is sufficient to use a harmonic potential V_v in equation (3):

$$V_v(r; s) = \frac{\hbar\omega_v(s)}{2}\left(\frac{v}{a_v}\right)^2. \tag{8}$$

Generalization to a Morse potential is straightforward.

The oscillator length is $a_v(s) = \sqrt{\hbar/m\omega_v(s)}$.

Because of the curvature of the reaction path, the translation–vibration coupling is not only due to the s-dependence of the parameters in (8) but also to centrifugal and Coriolis terms in the kinetic energy depending on the path of the curvature $C(s)$ [75].

Vibrational dynamics has been the subject of various investigations of hydrogen desorbing from metal surfaces [63, 76, 77]. The vibrational heating is well understood and the properties of the PES are well known. Although the bonding of hydrogen to the silicon surface is quite different from that to metal surfaces, one can expect the PES describing the vibrational dynamics at semiconductor surfaces to be similar apart from some details. The value of the curvature as well as a reduction of the vibrational frequency to about 25% at the transition state are taken from the *ab initio* calculations. We use the same parametrization as in (6).

4.5.4. Rotation. For the rotational potential we assume harmonic frustration of the rotations of adsorbed particles coming from harmonic forces on adsorbed atoms. We use the mass-scaled version

$$V_r(\vartheta, \varphi; s) = \frac{mr(s)^2}{2}\left(\omega_\vartheta^2(s)\cos^2\vartheta + \omega_\varphi^2(s)\sin^2\vartheta\cos^2\varphi\right). \tag{9}$$

4.5.5. Corrugation. The dominant effect of *surface corrugation* for normal incidence is a reduction of the sticking coefficient [68, 69]. The variation of the barrier height across the surface leads to a 'hole effect', i.e. a more or less geometrical decrease of the effective surface area available for sticking which is practically independent of the energy at low energies. From our investigations of the situation for H_2/Cu [68] we know that this effect can cause a reduction of about two orders of magnitude. Furthermore, the angular dependence of sticking will be influenced. In general for non-normal incidence the role of surface corrugation is more complex. The additional parallel momentum can lead to an enhancement or a suppression of the sticking coefficient, depending on the type of corrugation and the energy regime [69, 70].

In this calculation we assume only an 'energetic corrugation' of the potential where only the height and not the position of the barrier is varied along the surface. In this case the overall effect of corrugation is an approximately temperature-independent decrease of the sticking coefficient. We use the simple expression

$$V_c(\boldsymbol{y}; s) = V_{c1}(s)\left(1 - \cos\left(\frac{2\pi}{b_1}y_1\right)\right) + V_{c2}(s)\left(1 - \cos\left(\frac{2\pi}{b_2}y_2\right)\right) \tag{10}$$

with

$$V_{ci} = \frac{m}{\cosh^2(\lambda_c s)}\left(\frac{\omega_{ci}b_i}{2\pi}\right)^2 \qquad i = 1, 2. \tag{11}$$

The range of the corrugation perpendicular to the surface was taken to be $\lambda_c = 2$ Å^{-1}, the same for both directions, and equal to λ_p and similar to the value for H_2/Cu [68]. The

frequencies ω_{ci} can be estimated from an upper limit $\omega = 60$ meV for the 'rocking mode' of dihydrides observed in electron energy-loss spectroscopy experiments at high coverage [71–73] and a lower limit of $\omega = 5$ meV for the modes at the symmetric inter-dimer transition state normal to the dimers as found in *ab initio* calculations [36]. There are also two intermediate frequencies in the *ab initio* results at 15 meV (for the mode parallel to the dimers at the symmetric state) and 45 meV (for the asymmetric state). Since the precise nature of the transition state is not known yet, we chose two sets of frequencies which are fitted to angular distributions. It turns out that the two intermediate frequencies quoted above are both too high, yielding angular distributions that are too narrow (if the new data are taken into account, which lead to translational heating). But if they are reduced by about a factor of two: $\omega_{c1} = 8$ meV (for the modes parallel to the dimers) and $\omega_{c2} = 20$ meV (for the mode orthogonal to the dimers at the asymmetric inter-dimer state), one can obtain agreement with observed angular distributions (and also keyhole factors). This will be described in more detail in section 6.

5. Detailed balance

Before discussing the results of detailed dynamical calculations in the next subsection, we consider a general property of such results following from the principle of *detailed balance*. The original 2D model [34] was constructed so as to fulfil this principle in the presence of an adsorption barrier but the apparent absence of a potential drop after desorption.

In this section we derive mathematical consequences of detailed balance for sticking coefficients and desorption rates for our 7D model. The essential ingredient is time-reversal invariance leading to symmetry relations for the scattering matrix U:

$$U = \begin{pmatrix} L & S \\ D & R \end{pmatrix}. \tag{12}$$

Here S and D indicate sticking and desorption matrices with matrix elements

$$S(E)_{\boldsymbol{Qm},\boldsymbol{Pn}} \qquad D(E)_{\boldsymbol{Pn},\boldsymbol{Qm}} \tag{13}$$

where $\boldsymbol{n} = (n_p, n_v, l, m)$ and $\boldsymbol{P} = 2\pi\hbar(n_1, n_2)/L$ are the quantum numbers for lattice vibrations, molecular vibrations, rotations and parallel momenta (assuming periodic boundary conditions) on the gas side and $\boldsymbol{m} = (m_p, m_v, m_1, m_2)$ and $\boldsymbol{Q} = 2\pi\hbar(n_1, n_2)/L$ are the corresponding ones on the surface side of the barrier. For periodic surfaces, $\boldsymbol{P}$ and $\boldsymbol{Q}$ can only differ by a reciprocal-lattice vector $\hbar\boldsymbol{K}$. E is the total energy which is conserved in the reaction.

The total energy on the gas side (label g) consists of the translational energy $\varepsilon(p) = p^2/(2M)$ along the reaction path, the translational energy $\varepsilon(\boldsymbol{P}) = \boldsymbol{P}^2/(2M)$ parallel to the surface, the vibrational energy $\varepsilon_{\boldsymbol{n}} = \hbar\omega_p(n_p + 1/2) + \hbar\omega_v(n_v + 1/2)$ and the rotational energy $\hbar l(l+1)/(2mr^2)$:

$$E = E_g = \varepsilon(p) + \varepsilon(\boldsymbol{P}) + \varepsilon_{\boldsymbol{n}}. \tag{14}$$

On the surface side (label s) there is, besides an intrinsic energy E_s similar to that for the gas side, a binding energy $-B$:

$$E = E_s - B = \varepsilon(q) + \varepsilon(\boldsymbol{Q}) + \varepsilon_{\boldsymbol{m}} - B. \tag{15}$$

Here q is again the momentum along the reaction path and $\boldsymbol{Q}$ the momentum parallel to the surface. Conservation of total energy is described by

$$E_g = E_s - B. \tag{16}$$

As already mentioned in the last section, the quantum numbers on the surface side are not directly accessible by experiment. In order to eliminate unobservable details of the

intermediates, one considers sticking probabilities *summed* over and desorption probabilities *averaged* over the quantum numbers of the intermediates.

A typical sum of this kind is

$$s(\boldsymbol{P}, \boldsymbol{n}, E_g) = \sum_{Qm} |S(E_g)_{Qm,Pn}|^2 \tag{17}$$

which is the (initial-state-resolved) sticking probability of molecules starting in the state $\boldsymbol{P}, \boldsymbol{n}, E_g$ on the gas side.

Similarly one can define $d(\boldsymbol{P}, \boldsymbol{n}, E_g; T_s)\ \mathrm{d}E_g$, a (final-state-resolved) probability of desorption from a surface at temperature T_s into the state $\boldsymbol{P}, \boldsymbol{n}$, and an energy interval $[E_g\ (=E_s - B), E_g + \mathrm{d}E_g]$.

We assume equilibrium of the last intermediates with a Boltzmann distribution $\propto \exp(-\beta_s E_s)\ \mathrm{d}q$ (with $\beta_s = 1/(kT_s)$) of intermediate-state momenta in the interval $\mathrm{d}q$: the coupling of the last intermediates to the final states localized near adsorption sites is supposed to just provide this equilibrium. So we assume that there are no further slow intermediates which would occur if the desorption were e.g. diffusion limited.

The elimination of unobservable properties of the intermediates is then possible by taking into account that the desorption flux is $\propto |D(E)_{Pn,Qm}|^2 v(q)$ ($v(q)$ the velocity) and that $v(q)\ \mathrm{d}q = \mathrm{d}\varepsilon(q) = \mathrm{d}E_s = \mathrm{d}E_g$. Here the last equality is a consequence of the energy conservation.

The energy distribution of particles desorbing from a surface at temperature T_s into a state $\boldsymbol{P}, \boldsymbol{n}$ and an energy interval $\mathrm{d}E_g$ is then obtained from the equilibrium energy distribution (Z_s is the partition function for T_s)

$$\exp(-\beta_s E_s)\ \mathrm{d}E_s / Z_s = \exp(-\beta_s (E_g + B))\ \mathrm{d}E_g / Z_s \tag{18}$$

as

$$d(\boldsymbol{P}, \boldsymbol{n}, E_g, ; T_s) = \sum_{Qm} |D(E_s)_{Pn,Qm}|^2 \exp(-\beta_s (E_g + B))/(kT_s Z_s). \tag{19}$$

The basic ingredients of the so-called 'detailed balance' are symmetry relations following from time-reversal invariance. For surfaces with inversion symmetry they are

$$S(E)_{Qm,Pn} = D(E)_{Pn,Qm}. \tag{20}$$

If there is no inversion symmetry, the parallel momenta on the r.h.s. of this equation have to be replaced by their time-reversed (i.e. negative) values.

The simplest consequence of this symmetry relation and energy conservation is obtained if the Boltzmann-averaged state-resolved desorption probability is expressed in terms of the state-resolved sticking probability:

$$d(\boldsymbol{P}, \boldsymbol{n}, E_g; T_s) = s(\boldsymbol{P}, \boldsymbol{n}, E_g) \exp(-\beta_s (E_g + B))/(kT_s Z_s). \tag{21}$$

This relation says that deviations of the energy distribution of desorbing particles (at a substrate temperature T_s) from a Boltzmann distribution can be related to the state and energy dependence of sticking coefficients. In particular, sticking coefficients increasing (decreasing) with initial-state energy lead to heating (cooling) of desorbing particles with respect to T_s. This is something which can be checked experimentally.

The simplest check, of course, is obtained by summing the relation over the quantum numbers of the gas and integrating over all energies. Introducing the total desorption probability

$$d(T) = \sum \int \mathrm{d}E_g\ d(\boldsymbol{P}, \boldsymbol{n}, E_g, T) \tag{22}$$

($T = T_s = T_g$ is the common temperature of the surface and gas) and the thermally averaged sticking probability (Z_g is the corresponding partition function)

$$s(T) = \sum \int \mathrm{d}E_g \; s(\boldsymbol{P}, \boldsymbol{n}, E_g) \exp(-\beta E_g)/(kTZ_g) \tag{23}$$

we have

$$d(T) = s(T) \exp(-B/(kT)) \frac{Z_g}{Z_s}. \tag{24}$$

An equation like this can also be derived from the equilibrium condition of the kinetic equation for adsorption–desorption ($\mathrm{d}n_s/\mathrm{d}t = -\mathrm{d}n_g/\mathrm{d}t = sj_g - dj_s = 0$). It is clear from our derivation that $d(T)$ and $s(T)$ also describe non-equilibrium situations with non-vanishing $\mathrm{d}n_s/\mathrm{d}t = -\mathrm{d}n_g/\mathrm{d}t$.

For an experimental check one has to measure—besides the kinetic quantities $d(T)$ and $s(T)$—the thermodynamic quantity B.

In particular in the case of H_2/Si, the sticking coefficient is activated. One has approximately $s(T) \propto \exp(-\beta E_a)$ and similarly $d(T) \propto \exp(-\beta E_d)$. Hence one has approximately $E_d = E_a + B$.

Another quantity of interest is the dependence of the desorption flux into a volume element $\mathrm{d}^3\boldsymbol{p} = \mathrm{d}p\,\mathrm{d}^2\boldsymbol{P} = p_t^2\,\mathrm{d}p_t\,\mathrm{d}\Omega$ in momentum space on the total translational momentum $p_t = |\boldsymbol{p}|$ and angle θ. This is obtained essentially by summing $d(\boldsymbol{P}, \boldsymbol{n}, E_g, T)$ over the vibrational quantum numbers $\boldsymbol{n}$ for fixed total translational energy and θ.

We introduce polar angles in momentum space

$$\boldsymbol{p} = (p, \boldsymbol{P}) = p_t(\cos\theta, \cos\phi \sin\theta, \sin\phi \sin\theta) \tag{25}$$

and the total translational energy

$$\varepsilon_t = \varepsilon(p_t) = \frac{p^2 + \boldsymbol{P}^2}{2M} = \frac{p_t^2}{2M}. \tag{26}$$

After this we are able to introduce the p_t- and θ-dependent sticking and desorption probability averaged over the vibrational population at temperature $T_g = T_s = T$. Assuming isotropy in ϕ, the state-resolved sticking and desorption probabilities s and d depend only on the absolute magnitude $|\boldsymbol{P}| = p_t \sin\theta$ of the parallel momenta.

We introduce the sums

$$s(p_t, \theta) = \sum_{\boldsymbol{n}} s(p_t \sin\theta, \boldsymbol{n}, \varepsilon(p_t) + \varepsilon_{\boldsymbol{n}}) \exp(-\beta\varepsilon_{\boldsymbol{n}})/Z_g \tag{27}$$

and

$$d(p_t, \theta, T) = \sum_{\boldsymbol{n}} d(p_t \sin\theta, \boldsymbol{n}, \varepsilon(p_t) + \varepsilon_{\boldsymbol{n}} + B, T). \tag{28}$$

In these equations we have explicitly indicated the dependence of the total energy on $\boldsymbol{n}$ (besides the quantum numbers $\boldsymbol{P}$), since the averaging procedure has to be done for fixed translational energy but variable total energy.

Taking into account that the energy differential $\mathrm{d}E_g$ is given by $\mathrm{d}E_g = p\,\mathrm{d}p = p_t \cos\theta\,\mathrm{d}p$, one finds (as a consequence of detailed balance) another relation between desorption and adsorption fluxes:

$$d(p_t, \theta)\,\mathrm{d}E\,\mathrm{d}^2\boldsymbol{P} = s(p_t, \theta) \cos\theta p_t^3 \exp(-\beta(\varepsilon(p_t) + B)) \frac{Z_g}{Z_s}\,\mathrm{d}p_t\,\mathrm{d}\Omega \tag{29}$$

which is also a relation which can be checked experimentally.

6. Dynamical calculations

6.1. Introduction

Molecular dynamics involving hydrogen usually shows large *quantum effects*. For hydrogen on silicon even the zero-point energies of the Si lattice (of the order of 300 K) are about 30% of the highest thermal energies at 900 K. So for accurate results, quantum dynamical calculations are desirable. Naturally this strongly restricts the number of atoms which can be treated explicitly in the dynamics. Up to now in surface dynamics, maximally six degrees of freedom could be treated quantum mechanically [47, 49]. These were just the six coordinates of the hydrogen molecule on (static) Pd or Cu.

In our case the dynamics of the silicon lattice has to be taken into account. Even in the simplest approximation with only one lattice oscillator, the high excitation energies of this oscillator require about 20 to 25 additional channels which have to be saved somewhere else. If one omits either the rotational degrees (about 20 channels, taking symmetries into account) from the calculations or the corrugation (which also uses about 20 Fourier components), one ends up with a five-dimensional calculation. Note that it is not so much the dimension in coordinate space of the problem but the dimension in Hilbert space (the number of channels) which is relevant in the numerical procedure. The two 5D calculations just mentioned, for instance, need about the same number of channels (1000 to 3000) as the two 6D calculations for Pd and Cu.

Fortunately one can already obtain useful information by neglecting even more hydrogen degrees of freedom. For instance, the molecular vibrations and rotations as well as the corrugations involve much less energy than the translation along the reaction path and the lattice vibrations. Rotations and corrugations mainly reduce the sticking coefficient by an approximately constant 'keyhole factor'. Molecular vibrations are excited only at higher energies (above 0.2 eV). Hence the energy dependence of hydrogen–silicon sticking coefficients at lower energies can be described quite well by a 2D model involving only the centre-of-mass coordinate of the hydrogen molecule along the reaction path and a single lattice coordinate.

Calculations of this kind, indeed, gave the first quantum dynamical results concerning phonon-assisted sticking in H_2/Si [34, 84]. They were extended then to increasingly higher dimensions [9, 37, 42, 45, 92].

Finally, of course, to have a complete overview of the consequences of our 7D model one has to treat all seven degrees of freedom on an equal footing. If one were to do this straightforwardly by adding about 20 Fourier components to treat corrugation or about the same number of Legendre polynomials to treat rotations in addition to the 5D problems mentioned above, one would have forty to fifty thousand channels altogether. This is too much for the memory space of present-day computers.

In order to save memory space, we have introduced optimized basis states: 'breathing' oscillator states moving along 'quantum trajectories' [90, 91]. The application of these states in treating lattice vibrations in a harmonic model led to a great reduction of the number of channels needed for convergence [90]. The lattice vibrations in H_2/Si, however, are strongly anharmonic and the results were less promising in this case. Another example was the corrugation [91]. Here various approximations for the angular distribution in a 4D model with only 1D corrugation were compared with an 'exact' result obtained by using 15 Fourier coefficients. It turned out that an approximation with only three optimized basis states (neglecting the coupling between these states) gave a ten per cent accuracy. With five optimized basis states the deviation was about five per cent and with seven states about

one per cent. Furthermore, comparing 3D, 4D and 5D results without corrugation with corresponding results including an additional 1D corrugation, it turned out that the effect of corrugation was essentially multiplicative: the S-matrix was to a good approximation a product of the S-matrix of the non-corrugated model and a 'corrugation factor' depending little on dimension.

These results were obtained for a frequency ω_c of 20 meV. For lower frequencies the corrugation potential becomes more anharmonic and the convergence in the optimized basis states becomes worse. For the frequencies $\omega_c = 5$ meV and 8 meV mentioned above, the convergence is slow. A calculation with Fourier coefficients shows comparable convergence (seven coefficients are sufficient) and the factorization approximation still works well. So for the low frequencies, we calculate 7D results by comparing a 3D result without rotations and corrugation and a 5D result without rotations to obtain the corrugation factor; then we multiply a 5D result without corrugation by this factor to obtain the 7D result.

The time-independent coupled-channel problem is solved by propagating—instead of the Schrödinger matrices—two quantities (called the local reflection—*LORE*—and inverse transmission—*INTRA*) matrices along the reaction path. These matrices contain (besides periodic functions) only exponentially *decreasing* functions [64]. The *LORE* and *INTRA* matrices are sufficient to determine the scattering (reflection and transmission) matrix.

Sometimes, for instance for visualizing the results, it is desirable to know the wave function itself in coordinate space. This is possible, in principle, but requires the storage of the *LORE* and *INTRA* matrices along the whole reaction path [65]. For a hundred mesh points along the reaction path this would increase the memory needed by two orders of magnitude.

In order to visualize our results in terms of wave-function plots approximately, we therefore break our 7D model down to a number of 2D or 3D models containing maximally one additional degree of freedom besides the reaction and the lattice coordinate.

As examples we present 2D density plots in the subspace of the reaction coordinate s together with all other degrees of freedom obtained from such 2D or 3D calculations.

6.2. Calculations

6.2.1. Translation. We begin with adsorption and desorption wave functions in the 2D *translation–phonon* subspace obtained from 3D calculations (with translation, phonon and molecular vibration taken into account). The lattice as well as the molecule are assumed to be initially in their ground states. Figure 2 shows a density plot of such wave functions together with the model PES contour plot used for the calculation. The energy difference between adjacent contours is 0.1 eV. The kinetic energy of the incident molecule is 0.2 eV corresponding to the highest energy used in the beam experiments described above. The lattice is assumed to be initially in its ground state. In the experiments the temperature is slightly elevated by a few hundred degrees which leads to some admixture of excited phonons which, however, does not change the situation substantially. The incident molecule is almost completely reflected as indicated by the zeros in the density resulting from the interference between incident and reflected parts of the wave function. The small transmitted component is many orders of magnitude lower in intensity and is invisible in this plot. In a second example (figure 3) we show a corresponding plot for a desorption wave function starting with a translational energy of 0.1 eV on the barrier. During desorption a small part of the potential energy at the barrier (0.6 eV plus zero-point-energy contributions) above the asymptotic potential minimum is converted into centre-of-mass kinetic energy, but most of it remains as excitation energy in the lattice showing up as a large-amplitude oscillation of the wave function. In a more realistic calculation taking more degrees of freedom of the lattice into account, this oscillation will be

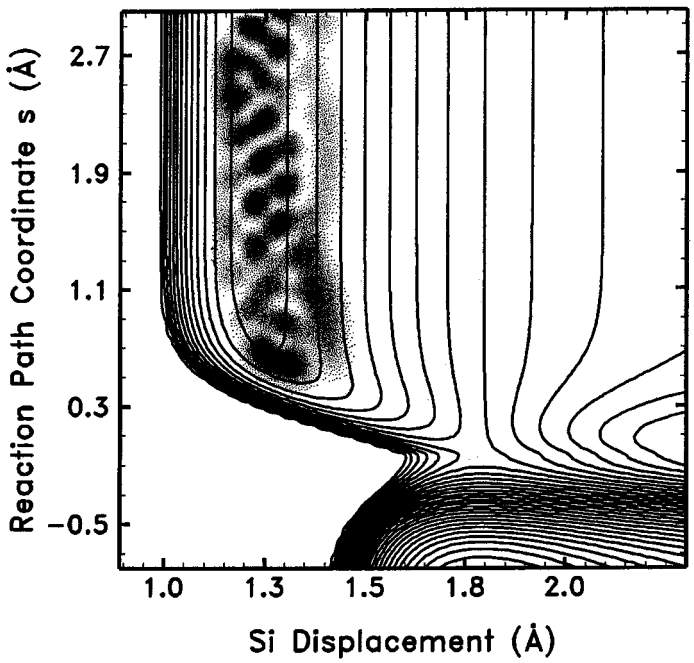

Figure 2. The adsorption wave function: a contour plot of the 2D model PES with the density of a 3D wave function (including molecular vibrations v) for a molecule incident from the gas side integrated over v. The incident particle is practically completely reflected (see the text).

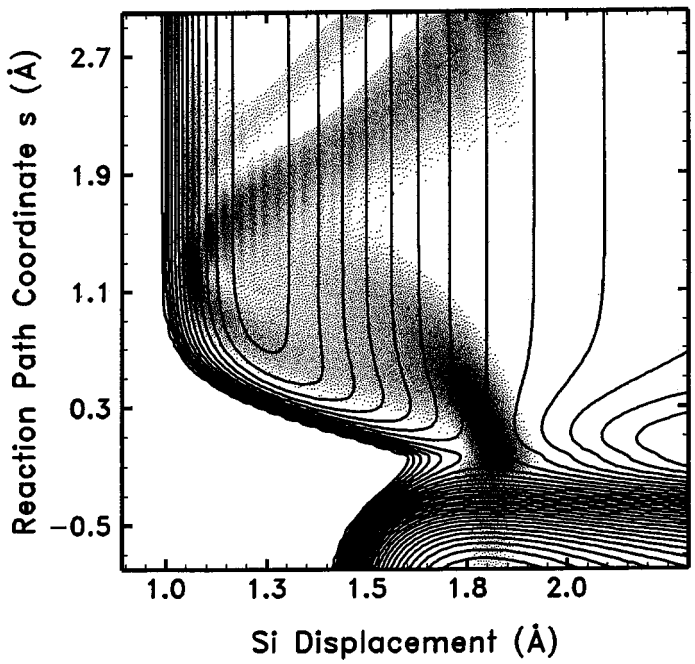

Figure 3. The desorption wave function: a contour plot of the 2D model PES with the density of a 3D wave function (including molecular vibrations v) for a molecule incident from the substrate side integrated over v.

damped out quickly: after the first bounce of the lower dimer atom with the next Si atom in the lattice, a large fraction of the initial energy will already be transferred to this atom and then to others.

These dissipative processes, however, have practically no influence on the motion of the hydrogen molecule any more. It is instructive to compare the desorption wave function with a number of trajectories shown in figure 4 describing the desorption process classically.

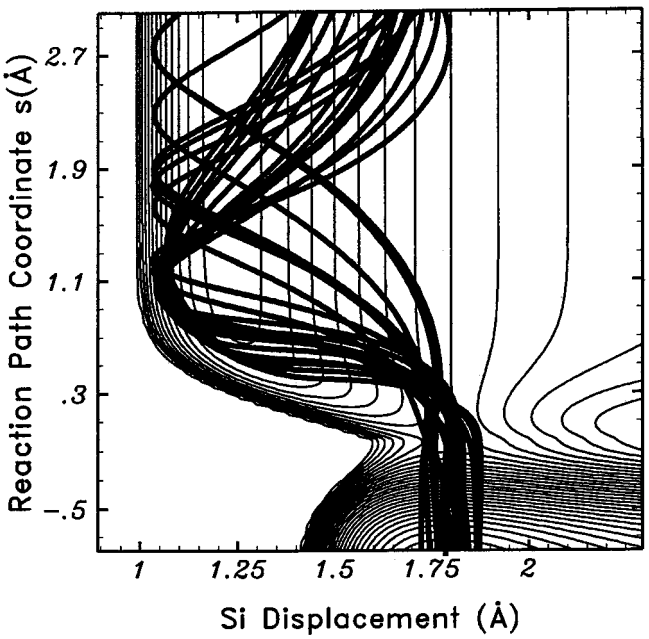

Figure 4. A number of classical trajectories describing desorption processes. In order to obtain a distribution of trajectories similar to the desorption wave function we consider trajectories with a number of different lattice energies on the barrier (between 0.01 eV and 0.03 eV) corresponding to the zero-point motion of the lattice.

The *ab initio* calculations of the PES have been extended to an *ab initio* molecular dynamics [48]. A group of 22 Si atoms in the slab calculations are considered mobile and the dynamics of these mobile atoms is treated using Newton's equations. For the details of these calculations we refer the reader to [48, 51]. It is instructive to look at three snapshots of a desorption event obtained from such a calculation (see figure 5). They clearly show the displacement of two silicon atoms in the course of the reaction.

In figure 6 we show the results of two 5D calculations of the dependence of molecular beam sticking coefficients on translational energy compared to experimental data. The corrugational effects were obtained with two rather low lateral frequencies of $\omega_{c1} = 0.005$ eV and $\omega_{c2} = 0.008$ eV. The effect of corrugation (as well as rotations) is a reduction of the sticking coefficients by roughly a factor of two. The combined effect of the two degrees of freedom in the product approximation of a 7D calculation mentioned above would lead to a result about a factor of two below the 5D value with rotations only. Low frequencies may occur in the context of symmetric transition states. For a symmetric inter-dimer state there will be an additional factor of two because of the two contributing dimer ends. This factor will compensate for the reduction because of corrugation. In both cases (intra- and inter-dimer) the results look similar to the 5D rotational result, which agrees with experiment.

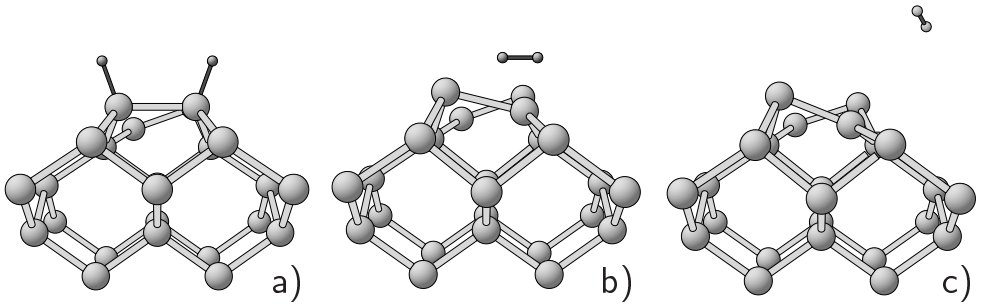

Figure 5. Three stages of a desorption process obtained from the classical *ab initio* molecular dynamics [48]: (a) adsorbed; (b) transition state; (c) desorbed.

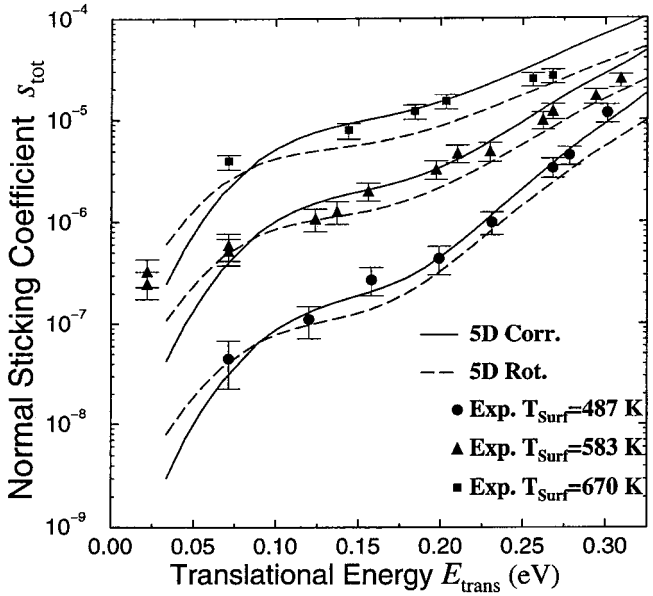

Figure 6. Calculated energy dependences of the sticking coefficients for several surface temperatures compared to experimental data. The strong increase above about 0.2 eV is due to vibrationally assisted sticking.

For two high lateral frequencies of 20 meV (perhaps representative of an asymmetric transition state) the absolute value of the sticking coefficients decreases by more than an order of magnitude. Also the angular distribution becomes too narrow compared to experiment. This will be discussed in more detail below (in subsection 6.2.5).

Another set of frequencies which would lead to agreement with experiment may be with one high frequency (perpendicular to the dimers) and one low frequency (parallel to the dimers) associated with an asymmetric inter-dimer state. In this case the absolute value of the sticking coefficients would be only slightly smaller than for the symmetric state discussed above. The angular distribution will be discussed below.

Another observable result associated with the translational energy is the desorption flux as a function of translational energy. In figure 7, we show the predictions of various approximations for this quantity as compared to the originally observed quasi-thermal distribution.

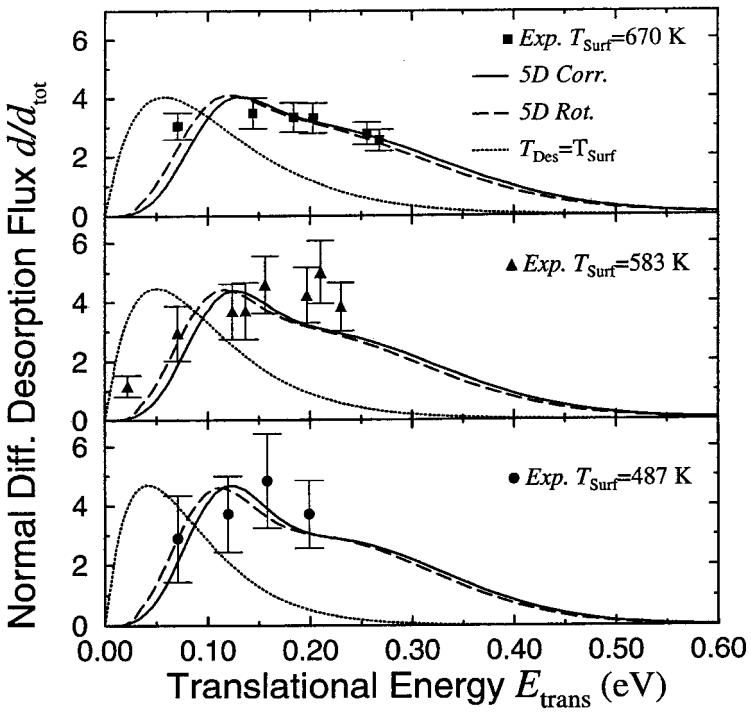

Figure 7. Normal desorption flux as a function of translational energy for three different surface temperatures. The experimental data points are obtained by applying detailed balance to molecular beam sticking data from [89]. For comparison a thermal desorption flux distribution is shown for all three surface temperatures as well.

All approximations agree within experimental accuracy and exhibit translational heating by a factor of two above thermal.

Direct measurements [12, 13, 100] show no translational heating. One has to bear in mind, however, that the molecular beam data [89] were taken at low coverages and that the presence of steps and defects with low barriers can influence the data strongly. In particular at higher coverages, half-filled inter-dimer sites [101, 102] produce low-barrier situations and corresponding contributions with thermal translational energy distributions in desorption. (Note, however, that models where these contributions completely dominate at higher coverages [101] will almost certainly lead to difficulties in explaining the observed vibrational heating (and probably also forward-peaked angular distributions) in desorption.)

All data, however, agree on the conclusion that the kinetic energy of desorbing molecules is considerably smaller than the adsorption barrier energy. So a large proportion of this energy has to go somewhere else (phonons or electrons). Applying detailed balance to this, one concludes that heating of the substrate must assist the sticking process. Since in our model there are no non-adiabatic couplings to electrons, we expect phonon-assisted sticking. For an accurate check of detailed balance it would certainly be desirable to have adsorption and desorption data for the same specimens and coverages.

6.2.2. Phonons (substrate). The predictions of the 7D model for experiments concerning the dependence of sticking coefficients on surface temperature are shown in figure 8 and figure 9 for various model dimensionalities and two different sets of lateral frequencies. The slope of

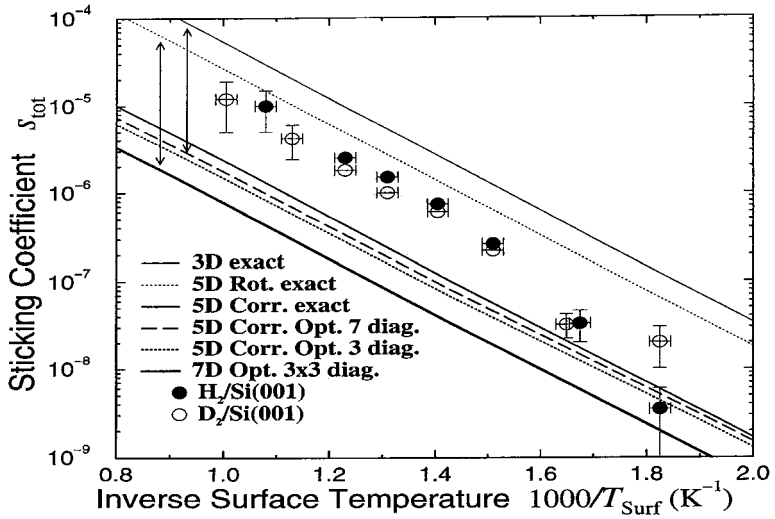

Figure 8. Sticking coefficient as a function of surface temperature T_{Surf} for various model dimensionalities. Both arrows indicate the reduction of the sticking coefficient due to the additional inclusion of a 2D corrugation with lateral frequencies equal to 20 meV. Note that the slope does not change very much for the different model dimensionalities. The experimental values are taken from [8].

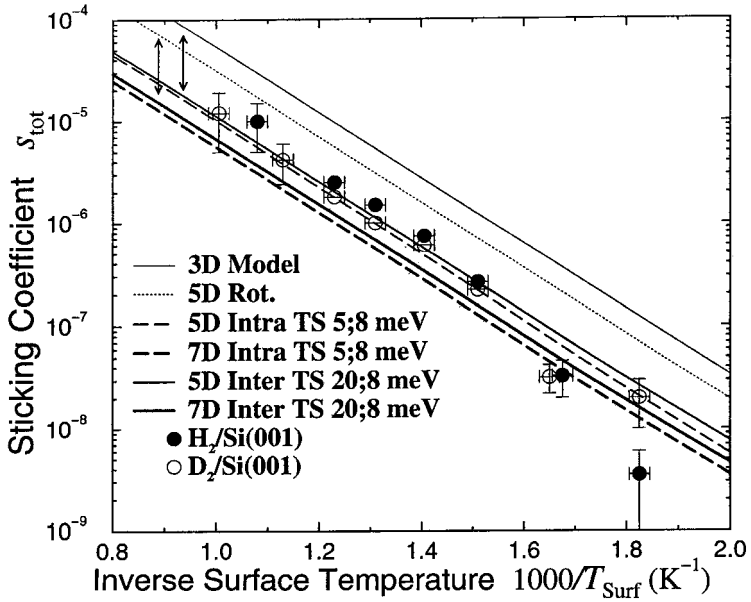

Figure 9. Calculated sticking coefficients for various model dimensionalities as functions of surface temperature T_{Surf} for lateral frequencies of 5 and 8 meV for the intra-dimer TS and for 20 and 8 meV for the inter-dimer TS. Experimental values are taken form [8]. Due to the lower lateral frequencies, the *keyhole* effect is not as strong as in figure 8.

the Arrhenius plot of the data corresponds to an effective barrier height of about 0.65 eV for Si(100). Note the absence of an isotope effect between H_2 and D_2.

6.2.3. Vibration. Let us now consider *molecular vibrations*. The physics behind the usually observed vibrational heating in desorption and the (via detailed balance) related vibrationally assisted sticking is a 'curved' reaction path with an early barrier in desorption (late in adsorption). For H_2 on Si, *ab initio* calculations of the PES lead to the typical 'elbow-shaped' equipotential contours of figure 10.

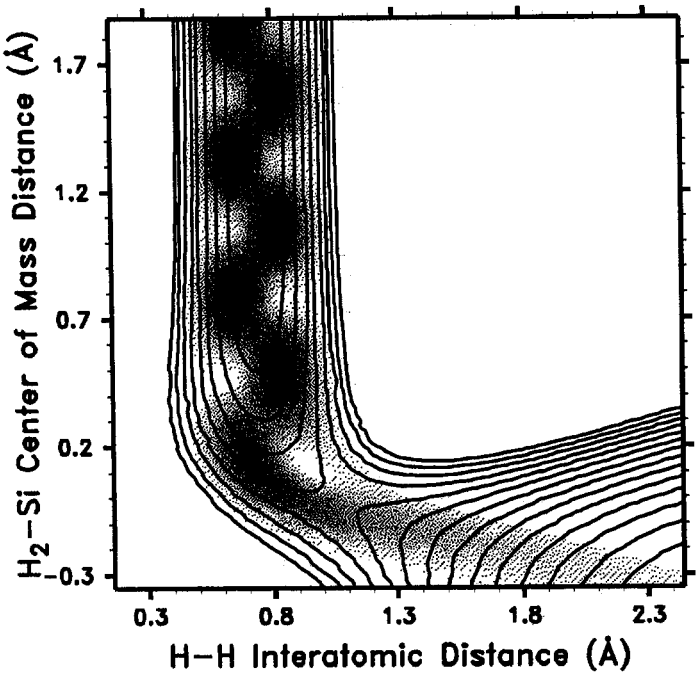

Figure 10. A density plot of a desorption wave as a function of the reaction coordinate s and the vibrational coordinate v obtained from a 3D calculation.

This figure also shows a density plot of a desorption wave function in the (s, v) subspace. The oscillation along the reaction path comes mathematically from a superposition of mainly the first excited state and the ground state of the molecular vibration with different phases corresponding to the different translational momenta of the two states.

Next we consider the distribution of molecular vibration energies of desorbing particles. Since the energy transfer to molecular vibrations is small and the hydrogen vibrational quanta are large, only the ground state and the first excited state need to be considered. Since there is a large isotope effect we consider HH, HD and DD isotopes. Our results are shown in figure 11. The results of 3D and 5D calculations for HH differ only little. We therefore only calculated 3D results (neglecting both lateral degrees of freedom of the hydrogen molecule) for the isotopes HD and DD. The vibrational quantum of H_2 molecules in the gas phase is $\omega_v = 516$ meV and for HD and D_2 $\omega_v = 450$ meV and $\omega_v = 371$ meV respectively. The vibrational population ratios that we find at a surface temperature of $T_s = 780$ K are $P_1/P_0 = 0.011$, 0.025 and 0.053 for H_2, HD and D_2 respectively. The ratio for the heavier molecules is larger due to their smaller vibrational quantum. These results are in good agreement with the vibrational state-resolved measurements of Kolasinski *et al* [10].

Related to vibrational heating in desorption is vibrationally assisted sticking in adsorption. This effect can be seen clearly in the molecular beam sticking data shown in figure 6. It starts around 0.2 eV translational energy and increases to about an order of magnitude around 0.3 eV.

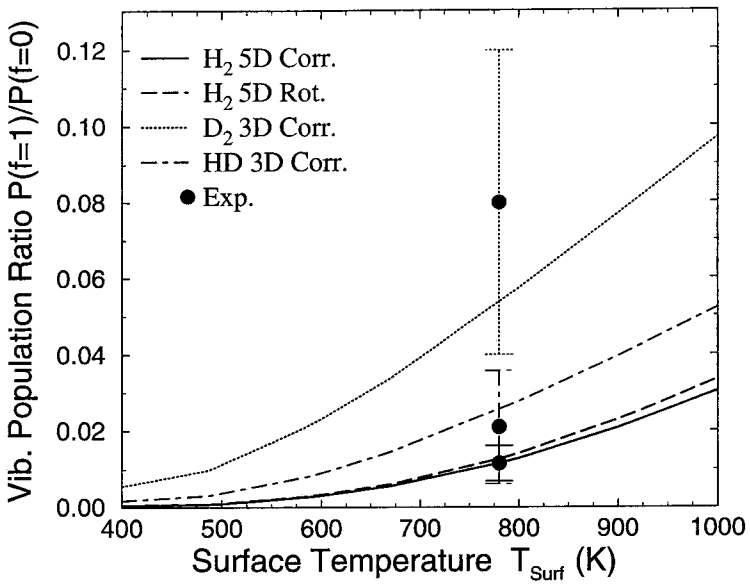

Figure 11. Vibrational population ratio of the first excited state compared to the ground state of the hydrogen molecules after desorption as a function of surface temperature T_{Surf}. The experimental data for $T_{\mathrm{Surf}} = 780$ K are taken from [10]. Note the strong isotope effect—in contrast to the phonon-assisted sticking.

Note that the change in translational energy is produced by an increase in nozzle temperature—which in turn is equal to the vibrational temperature of the beam.

Another consequence of the different vibrational frequencies together with the reduction of these values on the barrier is a difference in effective potential barrier for the various isotopes. As D_2 has the lowest frequency, it has the highest effective adsorption barrier. This would result in a smaller sticking coefficient in adsorption.

There is, however, a counter-effect from the corrugation. This leads to a zero-point energy of the vibrations of the hydrogen centre of mass parallel to the surface. Since this zero-point energy increases with decreasing distance from the surface, it leads to an increase of the effective barrier.

6.2.4. Rotation. Next we consider the of *rotations* in our 7D model. Here the situation is in some ways opposite to that for the vibrational degree of freedom. While the vibrational frequency *increases* from the barrier towards the gas side, the frequencies responsible for the frustrations of rotations *decrease to zero* towards the gas side. This leads to an adiabatic expansion in desorption and a corresponding cooling of the rotational degree of freedom. Figure 12 shows the parameters of the rotational Hamiltonian. In figure 13 the ϑ-dependence of a 3D wave function integrated over φ is plotted.

Figure 14 exhibits the results for the rotational energy distribution in desorption for the vibrational ground state and first excited state. The agreement with experiment [14] is good. The rotational energy distribution deviates from a Boltzmann distribution. Such an effect occurs also for other late-barrier systems (e.g. H_2/Cu), where the H–H distance on the barrier is expanded as compared to the gas phase. One then has two effects working in opposite directions: at low rotational energies one has *steering* leading to an increase of the sticking coefficients with decreasing j. The steering effect decreases with increasing j. At higher j,

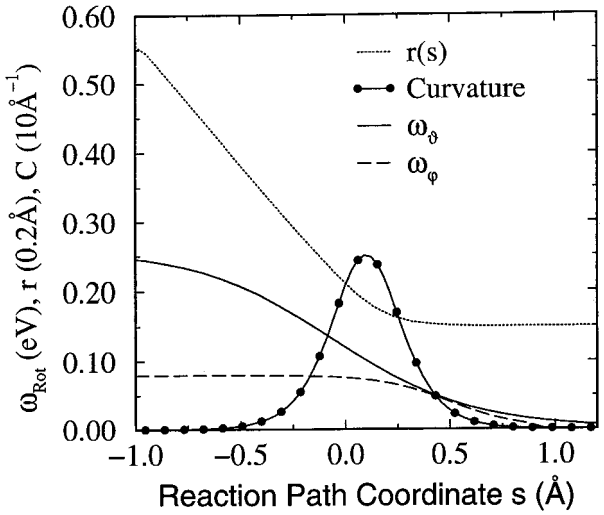

Figure 12. Rotational frequencies along the reaction path. The interatomic distance of the two hydrogen atoms and the reaction path curvature are shown as well.

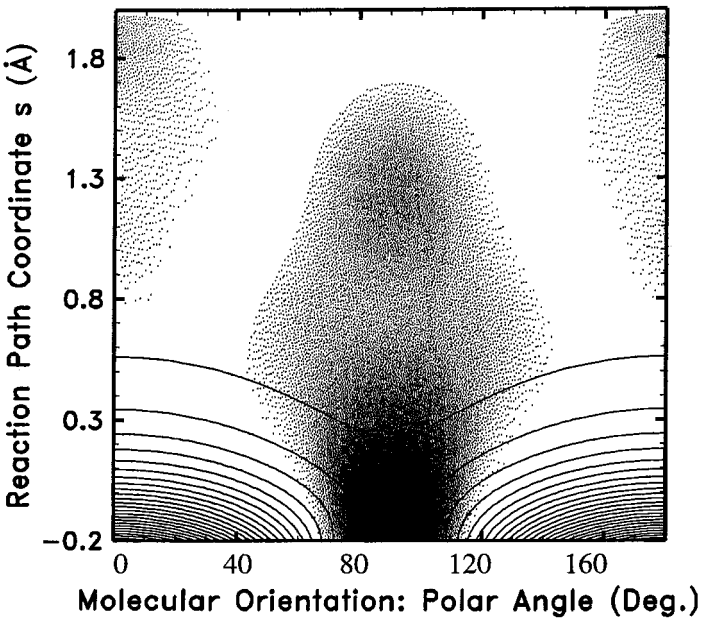

Figure 13. A density plot of the rotational ground-state desorption wave function for a translational energy of the ground state of 0.1 eV at the transition state.

however, the rotation–translation coupling increases: because of the expansion of the H–H distance towards the barrier, the rotational energy decreases; the excess energy is transferred to translational energy and can be used to overcome the barrier. This increases the sticking for larger j and (via detailed balance) reduces the rotational cooling.

In our model the polar frequency ω_ϑ is higher than the azimuthal frequency ω_φ. Hence the rotational frustration is stronger perpendicular to the surface than parallel to it. This kind of

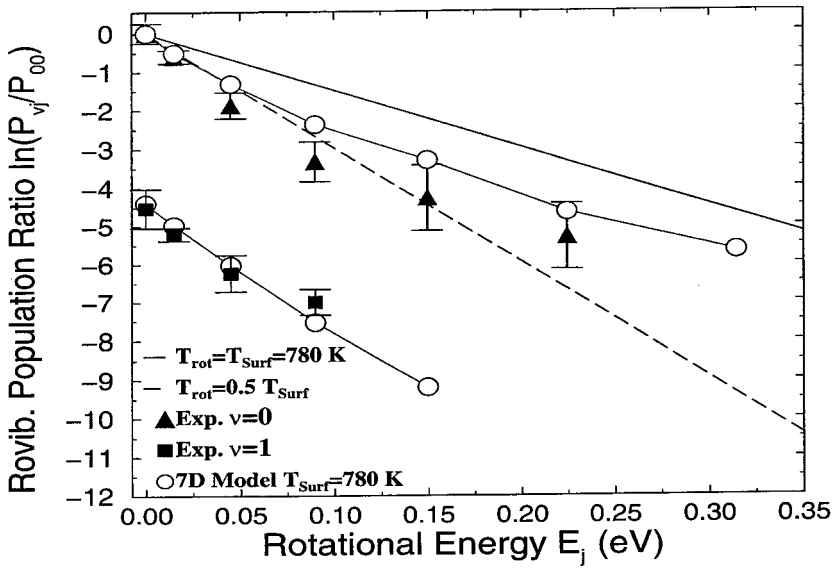

Figure 14. The rovibronic population ratio in desorption for a surface temperature $T_{\mathrm{Surf}} = 670$ K compared to experimental data from [14]. We find rotational cooling and a non-Boltzmann behaviour as in experiment [14]. All lines are guides to the eye.

anisotropy usually persists to some extent in desorption: the molecules desorb preferentially in a 'helicopter'-like fashion rather than in a 'cartwheel'-like one. Mathematically this can be described in terms of the so-called *alignment* coefficient

$$A(j, T_s) = \left\langle \frac{3j_z^2 - j^2}{j^2} \right\rangle_j = \left\langle \frac{3m^2 - j(j+1)}{j(j+1)} \right\rangle_j \tag{30}$$

lying between -1 and $3j/(j+1) - 1$. It is positive for helicopters and negative for cartwheels.

This quantity has not been measured yet for H_2/Si but we have calculated it for our model. The result is presented in figure 15.

6.2.5. Corrugation. Let us now consider the effect of *corrugation* first in a qualitative way. Figure 16 shows the desorption wave function obtained from a 3D calculation involving the two dominant coordinates s and x as well as one lateral coordinate y projected onto the two coordinates s and y (after integrating out the lattice coordinate x in the density).

Obviously only a small fraction of the unit cell contributes to desorption. This produces a more or less 'geometric' (and hence energy-independent) reduction of the desorption rate and a forward peaking of the angular distribution of desorbing particles. The corresponding adsorption wave function is not shown since it looks more complicated (because of the interfering reflected portions). But detailed balance tells us that the same geometric effect leads to a corresponding reduction of the sticking coefficient.

The effective barrier is, of course, also influenced by surface corrugation via contributions from the zero-point energy. To obtain agreement with experiment this has to be subtracted from the minimum energy barrier.

Desorbing molecules mainly propagate along paths which pass the barrier region close to the minimum-energy-barrier position [69]. In order to check whether our model potential describes the experimental situation properly in the vicinity of the minimum-energy path, we

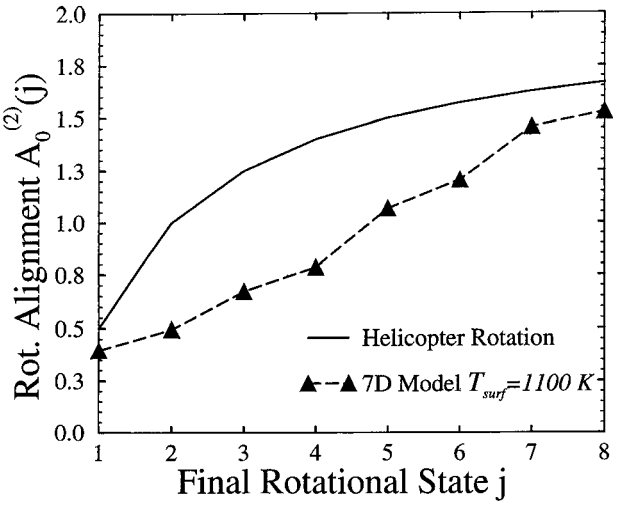

Figure 15. The predicted rotational alignment $A_0^{(2)}(j)$ of hydrogen molecules desorbing from Si(001) in our 7D model. The solid line indicates pure helicopter-like desorption. All lines are guides to the eye.

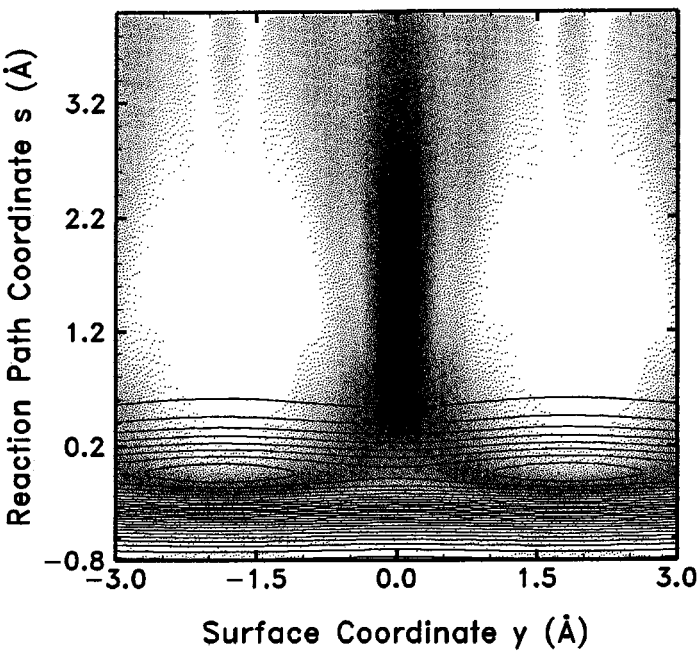

Figure 16. A density plot of a desorption wave as a function of the reaction coordinate s and the lateral coordinate y extending over one unit cell.

have also calculated the angular dependence of the sticking coefficients.

Experimentally, the first information about angular dependencies came from desorption data [18]. It turned out to be isotropic and forward peaked, $\propto \cos^n \theta$, with $3.9 \leqslant n \leqslant 5.2$ depending on the surface coverage.

The *ab initio* calculations on the other hand predicted a large anisotropy for the asymmetric transition state [36, 48] (40°–60° deviation from forward peaking, depending on the details of the calculations). This would lead to two separate peaks parallel to the dimer rows. Since, however, the data on angular distributions were obtained from multidomain surfaces, there would be an azimuthal averaging of this two-peak structure.

However, there are single-domain results [93, 102] showing azimuthal anisotropy and an even stronger forward peaking ($\propto \cos^{11}\theta$) *perpendicular* to the dimer rows. In the absence of detailed knowledge of the transition states involved and the corresponding corrugation parameters, we discuss the consequences of two sets of parameters which can describe the existing data.

The angular distribution depends on corrugation (influencing the distribution of parallel momenta) and the amount of translational heating (determining the distribution of normal momenta). The situation differs substantially between the earlier data indicating practically no translational heating and the recent molecular beam data [89, 92] indicating a normal translational energy in desorption of about twice the thermal energy.

In the absence of translational heating the angular distribution depends *strongly* on the corrugation. In our early attempts we took a frequency of $\omega_c = 60$ meV (equal to the dihydride rocking frequency) and were able to describe the observed angular distribution [18, 42]. We now know that this was fortuitous.

Taking the recent data on translational heating into account one finds forward peaking for low lateral frequencies ($\omega_{c1} = 0.005$ eV and $\omega_{c2} = 0.008$ eV) $\propto \cos^{11}\theta$ (practically the same for both frequencies), and for frequencies of 0.02 eV, $\propto \cos^{17}\theta$.

On a single-domain surface the averaging over dimer orientations can be avoided to some extent: perpendicular to the dimers the distribution should be symmetric and forward peaked; parallel to the dimers a superposition of two anisotropic distributions would be expected corresponding to the two oppositely buckled dimers in adjacent dimer rows. If the contributions from different dimers can be considered as independent, one would expect an angular dependence

$$s(\theta) \propto (\cos^{11}(\theta + \alpha) + \cos^{11}(\theta - \alpha))$$

for a dimer buckling angle at the transition state of α. This angle is not known, but for the reasonable value of $\alpha = 15°$ the above superposition is close to the observed dependence

$$s(\theta) \propto \cos^{3.2}(\theta).$$

According to recent low-coverage low-temperature data [94, 96] and *ab initio* results [99], the relevant transition state could be an inter-dimer state at one of two adjacent dimer ends. Parallel to the dimers the situation might be similar to that for the intra-dimer state: the frequency could be low, yielding a $\cos^{11}(\theta \pm \alpha)$ dependence which would have to be averaged as above. If there were something like a symmetric inter-dimer transition state, the situation could be completely equivalent to that for the symmetric intra-dimer state. The *ab initio* results indicate, however, an asymmetric state as the energetically lowest one. In this case the situation perpendicular to the dimers would be different: the frequency would be higher and the angular dependence more strongly peaked. The transition state would be tilted (perhaps by less than ±10° [99]) so there would be a superposition of two peaks. For $\omega_c = 0.02$ eV, for instance, one finds an angular dependence

$$s(\theta) \propto \cos^{17}(\theta).$$

The observed $\cos^{11}(\theta)$ dependence could then be produced by a superposition

$$s(\theta) \propto (\cos^{17}(\theta + \beta) + \cos^{17}(\theta - \beta))$$

with $\beta = 9°$ (see figure 17).

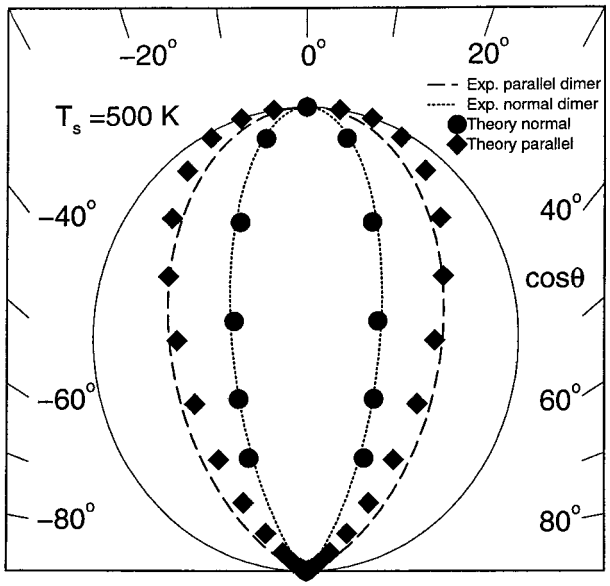

Figure 17. A polar plot of the angular distribution of hydrogen molecules desorbing from Si(100). The experimental data for deuterium desorption have been determined for coverages of $\theta_D = 0.6$ (solid line) and $\theta_D = 1.0$ (dashed line) [18]. The theoretical results are indicated by diamonds and circles. The $\cos\theta$ distribution is also shown as the dotted line for comparison.

7. Conclusions and discussion

We have presented the results of a comprehensive theoretical study of the reaction dynamics of molecular hydrogen with silicon surfaces—in particular, clean, single-domain, low-coverage Si(100).

A simple seven-dimensional model containing one substrate degree of freedom besides the translational coordinate, the molecular vibrations, rotations and surface corrugation is capable of describing *all* existing experimental data on molecular hydrogen adsorption and desorption, namely: the dependence of molecular beam sticking coefficients on translational energy, on the two angles of incidence, on the energies of molecular vibrations and rotations and on the surface temperature.

The corresponding desorption data are related to these data by the principle of detailed balance which is a consequence of our model.

The potential of the model is assumed to be a sum of seven terms related to the seven degrees of freedom. Each term contains five parameters: the values of the potential in the two asymptotic regions (gas or surface respectively) and the transition region, as well as the position and width of the transition region. The parameters in the asymptotic regions are usually taken from independent experiments. The transition region parameters are taken from *ab initio* calculations in many cases or used as fit parameters.

The availability of *ab initio* slab calculations has been enormously useful: they have demonstrated the existence of large lattice distortions in particular for the inter-dimer transition states of Si(100) and for Si(111) adatom adsorption. They have produced reasonable desorption barrier energies without requiring the invoking of defect-mediated processes (in contrast to cluster calculations). They have demonstrated the importance of steps in reducing adsorption barrier energies on Si(100).

On the other hand, as long as not *all* parameters can be obtained from *ab initio* data with sufficient accuracy, the microscopic interpretation of our model is ambiguous to some extent. The precise nature of the transition state, for instance, and the detailed form of the substrate relaxation are not known yet.

It is not obvious and to some extent even surprising, therefore, that a model as simple as that proposed in this paper is capable of describing a wealth of experimental data—and sometimes even predicting new effects.

Nevertheless there is a lot of room for improvement and further investigation. On the *ab initio* side, more details on the PES in the vicinity of the new inter-dimer adsorption and transition state are still lacking. Accurate values for adsorption barrier energies are badly needed (either from using improved functionals in DFT calculations, or using quantum Monte Carlo methods).

As regards dynamical model calculations, one may distinguish two types of improvement: either staying within the 7D model or extending the model by taking more degrees of freedom into account.

Within the 7D model the phonon potential V_p in the present model is too large in the asymptotic region (hydrogen in the gas phase) for large lattice amplitudes. Changes in the asymptotic region, of course, do not influence reaction rates. But the transition from the reaction region to the asymptotic region has to be smooth without influencing reaction rates. This, however, requires the introduction of several new parameters just to produce a null result, which we have not done so far. Large lattice amplitudes in the asymptotic region will not occur if dissipation in the lattice is taken into account. This, however, requires further lattice degrees of freedom in the model.

The postulated additivity of the potential in the various degrees of freedom is guaranteed in the harmonic approximation. Since the lattice coordinate, however, is assumed to be strongly anharmonic, there may be anharmonic couplings with other coordinates. For instance, modulations of the corrugation potential by the lattice coordinate may take place. In principle, anharmonic corrugation–rotation couplings may also occur (although we believe that in these variables the harmonic approximation works reasonably well).

The periodic corrugation of the potential in the adsorbed state has been neglected more or less completely. Again it can be expected to have little influence on the reaction rates. But if one is interested in what is going on after adsorption (or before desorption), the periodic part of the substrate potential for the adsorbed particles has to be taken into account.

With respect to further lattice degrees of freedom, one may distinguish two types.

The first one has been mentioned already in the context of dissipation, above. The primary atom hit by an incident hydrogen will soon transfer a large proportion of its energy to its next collision partner(s) in the lattice, induce a collision cascade and, finally, induce thermal equilibrium in the lattice. As long as there is a separation of timescales for desorption and, say, diffusion of particles and heat on the surface, the introduction of corresponding additional degrees of freedom will change the time constants for dissipation but not for adsorption/desorption.

There are, however, substrate degrees of freedom of a second type which interact more directly with the incident or desorbing hydrogen: there may be surface excitations which modulate the corrugation, for instance. Such excitations, we believe, deserve further attention.

Finally, there is the never-ending story of possible non-adiabatic electronic processes. In fact there are electronic excitations with an energy of the order of the adsorption barrier energy which in principle could be excited in desorption just as well as the lattice vibrations. We believe that the excitation probability, however, would be less because of the smallness of the electronic mass (which is just the origin of the adiabatic approximation).

Acknowledgments

It is a pleasure to thank many colleagues and friends, 'post-docs' and former graduate students for numerous stimulating discussions over the years and also for often communicating results before publication: U Höfer, M B Raschke, M Dürr, A Groß, P Kratzer, E Pehlke, R Russ, M Scheffler, R Brako, H Kasai, W A Diño, Y Miroa, J K Nørskov, D Doren and E A Carter. This research was supported by the Deutsche Forschungsgemeinschaft through Sonderforschungsbereich 338 (Projects C2 and C5) and the DAAD HSP-II programme.

References

[1] Sinniah K, Sherman M G, Lewis L B, Weinberg W H, Yates J T Jr and Janda K C 1989 *Phys. Rev. Lett.* **62** 567
Sinniah K, Sherman M G, Lewis L B, Weinberg W H, Yates J T Jr and Janda K C 1990 *J. Chem. Phys.* **92** 5700
[2] Wise M L, Koehler B G, Gupta P, Coon P A and George S M 1991 *Surf. Sci.* **258** 166
[3] Boland J J 1991 *Phys. Rev. Lett.* **67** 1539
Boland J J 1992 *J. Vac. Sci. Technol.* A **10** 2458
[4] Reider G A, Höfer U and Heinz T F 1991 *J. Chem. Phys.* **94** 4080
[5] Reider G A, Höfer U and Heinz T F 1991 *Phys. Rev. Lett.* **66** 1994
[6] Höfer U, Li L and Heinz T F 1992 *Phys. Rev.* B **45** 9485
[7] Bratu P and Höfer U 1995 *Phys. Rev. Lett.* **74** 1625
[8] Bratu P, Kompa K L and Höfer U 1996 *Chem. Phys. Lett.* **251** 1
[9] Bratu P, Brenig W, Groß A, Hartmann M, Höfer U, Kratzer P and Russ R 1996 *Phys. Rev.* B **54** 5978
[10] Kolasinski K W, Shane S F and Zare R N 1992 *J. Chem. Phys.* **96** 3995
Shane S F, Kolasinski K W and Zare R N 1992 *J. Chem. Phys.* **97** 3704
[11] Shane S F, Kolasinski K W and Zare R N 1992 *J. Chem. Phys.* **97** 1520
[12] Kolasinski K W, Nessler W, de Meijere A and Hasselbrink E 1994 *Phys. Rev. Lett.* **72** 1356
[13] Kolasinski K W, Nessler W, Bornscheuer K-H and Hasselbrink E 1994 *J. Chem. Phys.* **101** 7082
Kolasinski K W, Nessler W, Bornscheuer K-H and Hasselbrink E 1995 *Surf. Sci.* **331–333** 485
[14] Kolasinski K W 1995 *Int. J. Mod. Phys.* B **9** 2753
[15] Höfer U 1966 *Appl. Phys.* A **63** 533
[16] Raschke M B and Höfer U 1999 *Phys. Rev.* **59** 2783
[17] Flowers M C, Jonathan N B H, Liu Y and Morris A 1993 *J. Chem. Phys.* **99** 7038
[18] Park Y-S, Bang J-S and Lee J 1993 *Surf. Sci.* **283** 209
Park Y-S, Kim J-Y and Lee J 1993 *J. Chem. Phys.* **98** 757
[19] Widdra W, Yi S I, Maboudian R, Briggs G A D and Weinberg W H 1995 *Phys. Rev. Lett.* **74** 2074
[20] Morita Y, Miki K and Tokumoto H 1995 *Surf. Sci.* **325** 21
[21] Wu C J and Carter E A 1991 *Chem. Phys. Lett.* **185** 172
[22] Wu C J, Ionova I V and Carter E A 1993 *Surf. Sci.* **295** 64
[23] Wu C J, Ionova I V and Carter E A 1994 *Phys. Rev.* B **49** 13 488
[24] Nachtigall P, Jordan K D and Janda K C 1991 *J. Chem. Phys.* **96** 852
[25] Nachtigall P, Jordan K D and Sosa C 1994 *J. Chem. Phys.* **101** 8073
[26] Nachtigall P and Jordan K D 1995 *J. Chem. Phys.* **102** 8349
[27] D'Evelyn M P, Yang Y L and Suctu L F 1992 *J. Chem. Phys.* **96** 852
Yang Y L and D'Evelyn M P 1993 *J. Vac. Sci. Technol.* A **11** 2200
[28] Sheng J and Zhang J Z H 1992 *J. Chem. Phys.* **97** 596
[29] Jing Z and Whitten J L 1992 *Phys. Rev.* B **46** 9544
[30] Jing Z and Whitten J L 1993 *J. Chem. Phys.* **98** 7466
Jing Z and Whitten J L 1995 *J. Chem. Phys.* **102** 3867
[31] Jing Z, Lucovsky G and Whitten J L 1993 *Surf. Sci. Lett.* **296** L33
[32] Vittadini A, Selloni A and Casarin M 1993 *Surf. Sci.* **289** L625
[33] Vittadini A, Selloni A and Casarin M 1994 *Phys. Rev.* B **49** 11 191
[34] Brenig W, Groß A and Russ R 1994 *Z. Phys.* B **96** 231
[35] Sorescu D C, Thompson D L and Raff L M 1994 *J. Chem. Phys.* **101** 1638
[36] Kratzer P, Hammer B and Nørskov J K 1994 *Chem. Phys. Lett.* **229** 645
Kratzer P, Hammer B and Nørskov J K 1995 *Phys. Rev.* B **51** 13 432
[37] Kratzer P, Russ R and Brenig W 1996 *Surf. Sci.* **345** 125

[38] Pehlke E and Scheffler M 1995 *Phys. Rev. Lett.* **74** 952
[39] Vittadini A and Selloni A 1995 *Chem. Phys. Lett.* **235** 334
[40] Pai S and Doren D 1995 *J. Chem. Phys.* **103** 1232
[41] Li Guangwei, Chang Yia-Chung, Tsu R and Greene J E 1995 *Surf. Sci.* **330** 20
[42] Brenig W, Gross A, Höfer U, Kratzer P and Russ R 1996 *Springer Series in Solid State Science* vol 121 (Berlin: Springer) p 3
[43] Radeke M R and Carter E A 1996 *Surf. Sci.* **355** L289
[44] da Silva A J R, Radeke M R and Carter E A 1997 *Surf. Sci.* **381** L628
[45] Brenig W, Gross A, Höfer U and Russ R 1997 *Phys. Status Solidi* a **159** 75
[46] Vittadini A and Selloni A 1997 *Surf. Sci. Lett.* **383** L779
[47] Gross A, Wilke S and Scheffler M 1995 *Phys. Rev. Lett.* **75** 2718
[48] Gross A, Bockstedte M and Scheffler M 1997 *Phys. Rev. Lett.* **79** 701
[49] Kroes G J, Baerends E J and Mowrey R C 1997 *Phys. Rev. Lett.* **78** 3583
[50] Doren D J 1996 *Adv. Chem. Phys.* **95** 1
[51] Gross A 1998 *Surf. Sci. Rep.* **32** 291
[52] Jasinski J M, Meyerson B S and Scott B A 1987 *Annu. Rev. Phys. Chem.* **38** 109
[53] Yablonovitch E, Allara D L, Chang C C, Gmitter T and Bright T B 1986 *Phys. Rev. Lett.* **57** 249
Higashi G S, Chabal Y J, Trucks G W and Raghavachari K 1990 *Appl. Phys. Lett.* **56** 656
[54] Law J T 1959 *J. Chem. Phys.* **30** 1568
[55] Schulze G and Henzler M 1983 *Surf. Sci.* **124** 336
[56] Liehr M, Greenlief C M, Offenberg M and Kasi S R 1990 *J. Vac. Sci. Technol.* A **8** 2960
[57] Behm R J and Heinz K (ed) 1995 *Surface Reconstruction: Structure and Dynamics; Surf. Sci.* **337** 169
[58] Bischler U, Sandl P, Bertel E, Brunner T and Brenig W 1993 *Phys. Rev. Lett.* **70** 3603
[59] Polanyi J C and Wong W H 1969 *J. Chem. Phys.* **51** 1439
[60] Himpsel F J 1990 *Surf. Sci. Rep.* **12** 1
[61] Takayanagi K, Tanishiro Y, Takahashi S and Takahashi M 1985 *Surf. Sci.* **164** 367
[62] Hofacker G L 1963 *Z. Naturf.* a **18** 607
[63] Brenig W and Kasai H 1989 *Surf. Sci.* **213** 170
[64] Brenig W and Russ R 1994 *Surf. Sci.* **315** 195
[65] Brenig W, Groß A and Russ R 1995 *Z. Phys.* B **97** 311
[66] Allan D C and Mele E J 1984 *Phys. Rev. Lett.* **53** 826
[67] Bilz H and Kress W 1978 *Phonon Dispersion Relations in Insulators* (Berlin: Springer)
[68] Groß A, Hammer B, Scheffler M and Brenig W 1994 *Phys. Rev. Lett.* **73** 3121
[69] Groß A 1995 *J. Chem. Phys.* **102** 5045
[70] Darling G R and Holloway S 1994 *Surf. Sci.* **304** L461
[71] Schaefer J A, Stucki F, Anderson J A, Lapeyre G J and Göpel W 1984 *Surf. Sci.* **140** 207
[72] Froitzheim H, Köhler U and Lammering H 1985 *Surf. Sci.* **149** 537
[73] Tautz F S and Schaefer J A 1998 *J. Appl. Phys.* **84** 6636
[74] Brenig W, Brunner T, Groß A and Russ R 1993 *Z. Phys.* B **93** 91
[75] Rankin C C and Light J C 1969 *J. Chem. Phys.* **51** 1701
[76] Harris J, Holloway S, Rahman T S and Yang K 1988 *J. Chem. Phys.* **89** 4427
[77] Küchenhoff S, Brenig W and Chiba Y 1991 *Surf. Sci.* **245** 389
[78] Dabrowski J and Scheffler M 1992 *Appl. Surf. Sci.* **56–58** 15
[79] Wolkow R A 1994 *Phys. Rev. Lett.* **68** 2636
[80] Bullock E L, Gunella R, Patthey L, Abukawa T, Kono S, Natoli C R and Johansson L S O 1995 *Phys. Rev. Lett.* **74** 2756
[81] Krüger P, Mazur A, Pollmann J and Wolfgarten G 1986 *Phys. Rev. Lett.* **57** 1468
[82] Chabal Y J and Raghavachari K 1984 *Phys. Rev. Lett.* **53** 282
Chabal Y J and Raghavachari K 1985 *Phys. Rev. Lett.* **54** 1055
[83] Nachtigall P, Jordan K D, Smith A and Jónsson H 1996 *J. Chem. Phys.* **104** 148
[84] Luntz A C and Kratzer P 1996 *J. Chem. Phys.* **104** 3075
[85] Vittadini A and Selloni A 1995 *Phys. Rev. Lett.* **75** 4756
[86] Cho K, Kaxiras E and Joannopoulos J D 1998 *Phys. Rev. Lett.* **79** 5078
[87] Penev E, Kratzer P and Scheffler M 1999 *J. Chem. Phys.* **110** 3986
[88] Tokumoto H and Iwatsuki M 1993 *Japan. J. Appl. Phys.* **32** 1368
[89] Dürr M, Raschke M B and Höfer U 1999 *J. Chem. Phys.* **111** 10 411
[90] Brenig W, Brako R and Hilf M F 1996 *Z. Phys. Chem.* **197** 237
[91] Brenig W, Hilf M F and Brako R 2001 *Surf. Sci.* **469** 105

[92] Hilf M F and Brenig W 2000 *J. Chem. Phys.* **112** 3313
[93] Höfer U and Dürr M 2001 *PhD Thesis* TU Munich
[94] Biedermann A, Knoesel E, Hu Z and Heinz T F 1999 *Phys. Rev. Lett.* **83** 1810
[95] Raschke M B and Höfer U 1999 *Appl. Phys.* B **68** 649
[96] Dürr M, Raschke M B, Pehlke E and Höfer U 2001 *Phys. Rev. Lett.* at press
[97] Pehlke E and Kratzer P 1999 *Phys. Rev.* B **59** 2790
[98] Kratzer P *et al* 1998 *Phys. Rev. Lett.* **81** 5596
[99] Pehlke E 2000 *Phys. Rev.* B **62** 12 932
[100] Pusel A, Wetterauer U and Hess P 1998 *Phys. Rev. Lett.* **81** 645
[101] Zimmermann F M and Pan X 2000 *Phys. Rev. Lett.* **85** 618
[102] Dürr M 2000 *PhD Thesis* TU Munich